Separating freshwater flux effects on ENSO in a hybrid coupled model of the tropical Pacific

Chuan Gao[1,2,3] · Rong-Hua Zhang[1,2,3] · Kristopher B. Karnauskas[4,5] · Lei Zhang[4] · Feng Tian[1,2,3]

Abstract

Freshwater flux (FWF) at the sea surface, defined as precipitation minus evaporation, is a major atmospheric forcing to the ocean that affects sea surface salinity (SSS) and buoyancy flux (Q_B). Physically, there exist two pathways through which interannual FWF variability can affect the ocean: one through SSS and the other through Q_B. The roles of the interannual FWF variability in modulating the El Niño-Southern Oscillation (ENSO) through its effects on SSS or Q_B are separately examined using a hybrid coupled model (HCM) of the tropical Pacific; its ocean component is a layer model in which the topmost layer (the first layer) is treated as a mixed layer (ML) whose depth (H_m) is explicitly predicted using an embedded bulk ML model with H_m being directly affected by Q_B, whereas in level ocean models, Q_B does not have a direct and explicit effect on H_m. Four experiments are conducted using the HCM that is designed to illustrate the effects of these processes on coupled simulations systematically. It is demonstrated that interannual FWF variability serves as a positive feedback on ENSO through its collective effects on both SSS and Q_B. Individually, the interannual FWF effect through SSS accounts for about 80% in terms of ENSO amplitude in the Niño 3.4 area, while that through buoyancy flux accounts for about 26%. This indicates that ocean models without explicitly taking into account the direct FWF effect on Q_B (typically in level ocean models) could underestimate the positive feedback on ENSO compared with layer ocean models in which the FWF effects are collectively represented on both SSS and Q_B. Further implications for model biases associated with FWF effects are discussed.

Keywords Freshwater flux effects · Sea surface salinity · Buoyancy flux · Feedbacks on ENSO · Layer and level ocean models

1 Introduction

The El Niño-Southern Oscillation (ENSO), centered in the tropical Pacific, is the strongest interannual signal of the climate system (Bjeknes 1969), and it plays an important role in climate change and extreme climate disaster with ecological consequences (Latif and Keenlyside 2009). ENSO is an air-sea interaction phenomenon, whose coupling is realized through the flux exchanges among momentum, energy and water at the sea surface (Willebrand 1993). Three major atmospheric driving forces to the ocean are fluxes of momentum, heat and freshwater, which act to produce and modulate ENSO (e.g., Zhang and Busalacchi 2009a). Indeed, ENSO has been observed to exhibit modulations and diversity (Capotondi et al. 2015; Chen et al. 2015). Many climate models can simulate ENSO variations with varying success, but biases still persist in simulations of the mean state and interannual variability, including the frequency, amplitude and structure of ENSO (Ren et al. 2016). Note that the existing biases in ENSO simulation and prediction are strongly model dependent (Zhang and Gao 2016). In the past, many studies have emphasized the forcing effects of wind stress and heat flux (Waliser et al. 1994; Xie and Philander 1994); the atmospheric freshwater flux (FWF) forcing effect on the

✉ Rong-Hua Zhang
  rzhang@qdio.ac.cn

1 CAS Key Laboratory of Ocean Circulation and Waves, Institute of Oceanology, and Center for Ocean Mega-Science, Chinese Academy of Sciences, Qingdao 266071, China

2 Pilot National Laboratory for Marine Science and Technology, Qingdao 266237, China

3 University of Chinese Academy of Sciences, Beijing 10029, China

4 Department of Atmospheric and Oceanic Sciences, University of Colorado, Boulder, CO, USA

5 Cooperative Institute for Research in Environmental Sciences, University of Colorado, Boulder, CO, USA

ocean has been less focused in studies of ENSO modulations in the coupled system.

In the tropical Pacific, FWF at the sea surface, here defined as precipitation (P) minus evaporation (E), written as FWF = $P - E$, undergoes strong interannual variability, which is closely related to ENSO (Vialard et al. 2002; Wu et al. 2010; Zhi et al. 2015). During El Niño phase, for example, a pronounced positive FWF anomaly occurs in the central equatorial Pacific where the combination of climatological warm SSTs with positive SST anomalies maximizes convection and rainfall. Conversely, during La Niña phase, there is an obvious negative FWF anomaly in the central equatorial Pacific as the cold tongue extends further westward along with the warm pool convection contracting further to the west. FWF anomalies appear as atmospheric responses to ENSO, but simultaneously could have a feedback on ENSO (Zhang et al. 2015, 2019).

Physically, a FWF feedback on ENSO can be realized through its effects on sea surface salinity (SSS) and buoyancy flux (Q_B; Zhang and Busalacchi 2009a). Firstly, FWF directly affects the upper ocean salinity, which is an important field affecting stratification and vertical mixing (Miller 1976; Zheng and Zhang 2015). For example, the barrier layer resulting from FWF and salinity stratification in the warm pool can isolate the warm water in the upper ocean by inhibiting the subsurface cold waters entrained into the mixed layer (ML), and thus reduce the vertical mixing (Maes et al. 2002). Previous studies show that variations in FWF and the related SSS effects play an important role in the climate mean state and variability in the tropical Pacific, through affecting the horizontal pressure gradient, vertical stratification and mixing (Kessler 1999; Cravatte et al. 2009). Secondly, FWF is one part of Q_B, which has a direct effect on the ML dynamics. Because ML formulation is related to the wind stirring and the net buoyancy flux in the tropical Pacific, Q_B partially determines the turbulent kinetic energy balance in the ML and thus the entrainment of subsurface waters at base of the ML (Chen et al. 1994). So, Q_B is a field that directly determines the mixing in the upper ocean (Lumpkin and Speer 2007) and subsurface water entrainment into the mixed layer (Lupton et al. 1985), thus affecting the mixed layer depth (MLD). In terms of FWF role, the two different ways exist in which ENSO can be modulated through its effects on SSS and Q_B, respectively. However, it is difficult to distinguish the roles played by interannual FWF variability in modulating ENSO either through its effects on SSS or Q_B based on observation; model simulations can be conducted to address these issues.

Large uncertainties exist in representing the FWF effects in ocean models (Kang et al. 2017), which strongly depend on model formulations. For example, the simulated SSS structure is found to be quite sensitive to the ways the FWF

forcing is represented (Vialard and Delecluse 1998). Coupled models used in the Intergovernmental Panel for Climate Change 4th Assessment Report (IPCC AR4) show large model biases that still exist in simulations of SSS mean state and interannual variability (Delcroix et al. 2011), which is very sensitively dependent on the way FWF-related feedback processes are represented in ocean models.

The ocean models can be classified into level ocean models and layer ocean models (e. g., Chen et al. 1994; Zhu and Zhang 2018). One difference in these model constructions lies in the way the atmospheric forcing fields (including FWF) are affecting the upper ocean, and the surface mixed layer is represented and realized in simulation. For example, in the level ocean models [e. g., the version 5 of Modular Ocean Model (MOM5) developed at GFDL/NOAA], the model layer depth and thickness of each layer (including the topmost surface layer) are fixed to be constant; the MLD is not a prognostic variable and is not directly affected by FWF and Q_B. The well mixed layer at the sea surface is realized in the model by coefficients-based mixing effects of atmospheric forcings as follows. The atmospheric forcing is first applied to the topmost model level with a fixed thickness (say 10 m), and then penetrated vertically down to the subsurface level based on the vertical mixing coefficient estimated by the turbulent closure model (e.g., Large et al. 1994). On the other hand, in the layer ocean models in which the first layer is treated as a mixed layer determined by a bulk mixed layer model, Q_B can directly affect ML, whose thickness is allowed to vary in space and time (Chen et al. 1994). As such, the atmospheric forcing effects are homogeneously distributed over the whole mixed layer in the layer model. As such, the different mixed layer formulations in the layer and level ocean models affect the way the atmospheric forcing is represented, and thus affect the upper layer ocean simulations. It is therefore important to understand the sensitivity to ways the effects of atmospheric forcing fields including FWF are adequately represented in ocean and coupled modeling.

Our previous work has investigated the modulation of FWF on ENSO using a hybrid coupled model (HCM) of the tropical Pacific (Zhang and Busalacchi 2009a). The HCM consists of an ocean general circulation model (OGCM) and simplified atmospheric models. The OGCM, originally developed by Gent and Cane (1989), is a sigma coordinate layer model in which the first layer is assigned to be a mixed layer, whose depth is explicitly and directly affected by Q_B as represented by a bulk ML model (Chen et al. 1994). The layer OGCM takes into account the mixed layer dynamics and explicitly predicts MLD variation; this is contrasted to level models (e. g., the MOM5) in which the effect of Q_B on MLD is not explicitly accounted for. The layer ocean model with the bulk ML explicitly represented is then coupled to a simplified atmospheric model consisting of three

components: wind stress anomaly is calculated using a statistical model constructed from singular value decomposition (SVD) analysis (Zhang et al. 2006); heat flux is calculated from an advective atmospheric mixed layer (AML) model (Seager et al. 1995); interannual variation of FWF is calculated using a statistical model that is also constructed from SVD method (Zhang and Busalacchi 2009a). Here, the HCM is used to illustrate the roles of interannual FWF variability in modulating ENSO through its effects either on SSS or Q_B.

Based on our previous studies, the oceanic processes responsible for ENSO modulations induced by interannual FWF variability can be summarized as follows. During El Niño, a warm SST anomaly is observed in the eastern and central equatorial Pacific, accompanied with a positive FWF anomaly in the western and central equatorial Pacific, which directly affects SSS and Q_B, respectively. It further decreases the density with shoaling of the mixed layer, which strengthens the vertical stratification and weakens the entrainment of subsurface waters into mixed layer, sequentially weakening vertical mixing. These oceanic processes induced by the positive FWF anomaly further strengthen the warm SST anomaly, which in turn induces atmospheric responses in the coupled air-sea system, producing a positive feedback on ENSO (Zhang et al. 2015). Correspondingly, there exist two influence pathways which can be induced by interannual FWF variability on the ocean: one through SSS and the other through Q_B, respectively.

However, the individual role of each influence pathway played in the ENSO modulations has not been illustrated and the related effects have not been quantified. In order to quantitatively and clearly illustrate differently represented freshwater flux effects on ENSO, four experiments are conducted using the HCM to isolate each effect individually, in which SSS and/or Q_B can be affected by interannually varying and climatological FWF effects, respectively. Some specific questions are to be clarified from the four experiments: What are the biases induced by differently represented interannual FWF variability in the HCM? How can ENSO be quantitatively modulated by interannually varying FWF effects on SSS and Q_B, respectively? Does ENSO amplitude modulation collectively induced by FWF effects on SSS and Q_B both change linearly with that individually induced by the effect on SSS or Q_B, respectively? What are possible biases in simulations using level ocean models that can be related to interannual FWF forcing-induced effect on the ocean through the Q_B pathway compared with layer ocean models?

This paper is organized as follows. Section 2 describes the model used and the experimental design. Section 3 illustrates the model performance and effects on ENSO induced by interannually varying FWF. Section 4 demonstrates the effects on ENSO individually induced by FWF through the SSS pathway or Q_B pathway, respectively. The summary and discussion are presented in Sect. 5.

2 Model description and experimental design

To separately and clearly quantify the roles of interannual FWF variability in modulating ENSO through its effects either on SSS or Q_B, four experiments are conducted using a hybrid coupled model (HCM) with differently represented FWF effects on the ocean through SSS or Q_B. The model used and experimental design are briefly described in this section.

2.1 Description of the hybrid coupled model

The HCM used here consists of a layer ocean general circulation model (OGCM) and simplified atmospheric models. A schematic diagram of the HCM is shown in Fig. 1. The atmospheric models which determine the atmospheric surface forcings to the ocean include a statistical atmospheric wind stress anomaly model, an advection atmospheric mixed layer model (AML) for calculating heat flux (Murtugudde et al. 1996; Seager et al. 1995) and a statistical FWF anomaly model, respectively. The OGCM, the AML and the HCM all have been used extensively in our previous studies of the tropical Pacific (e.g., Karnauskas and Busalacchi 2009; Karnauskas et al. 2008).

The OGCM is a layer model originally developed by Gent and Cane (1989) for the upper ocean. It adopts a reduced gravity approximation based on σ coordinate in the vertical direction, divided into 20 layers; the first layer is a mixed layer. One main feature with the OGCM includes an embedded bulk model for the mixed layer, whose depth is explicitly predicted (Chen et al. 1994), a better representation of the mixed layer dynamics (Zhang and Zebiak 2002). As constructed, the bulk mixed layer model is used to determine the MLD (the thickness of the first layer). There are 19 layers below the mixed layer, which are determined by σ coordinate, with the thicknesses of 2–10 layers being between 5 and 10 m. Further improvements have been made in the OGCM. For example, the mixing processes in the upper ocean consist of Kraus-Turner mixed layer model (Chen et al. 1994) and Price dynamic instability model (Kraus and Turner 1967; Price et al. 1986). Thus, the model can well simulate the three major processes of vertical turbulent mixing, including wind stirring, shear instability and convective instability, respectively. Additionally, the optimized spatial-varying coefficient of wind stirring based on observation is adopted (Zhu and Zhang 2018), which can improve the simulation of MLD.
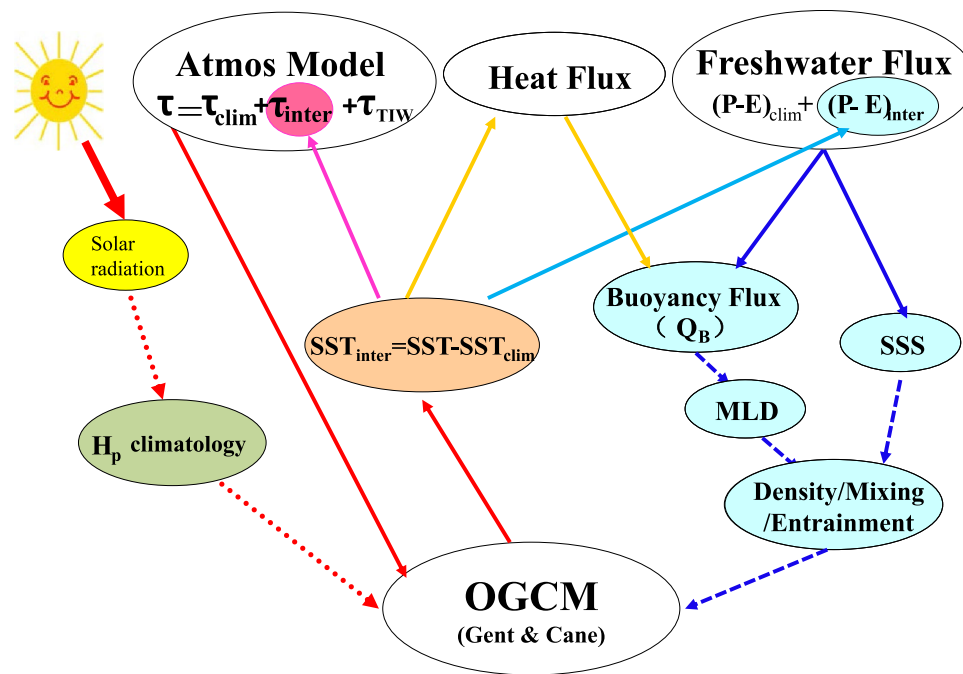
Fig. 1 A schematic diagram showing the components of HCM to illustrate the effect of FWF in the tropical Pacific air-sea coupled system. The HCM consists an ocean general circulation model (OGCM) and simplified atmospheric models. The atmospheric forcing fields to the OGCM include three parts: wind stress, heat flux and FWF. The wind stress field is written as $\tau = \tau_{clim} + \tau_{inter} + \tau_{TIW}$, which consists of the seasonal climatology part (τ_{clim}), interannual wind stress anomalies (τ_{inter}) calculated using interannual SST anomalies, and tropical instability wave (TIW)-induced wind stress perturbations (τ_{TIW}). The heat flux is calculated using the advective atmospheric mixed layer (AML) model developed by Seager et al. (1995). The FWF filed is written as FWF = (P − E)$_{clim}$ + (P − E)$_{inter}$, in which (P − E)$_{clim}$ is the seasonal climatology part and (P − E)$_{inter}$ is interannual anomalies part calculated using a statistical model from interannual SST anomalies. The fields directly influenced by FWF on the ocean include SSS and buoyance flux (Q$_B$), which together affect the ocean density, mixing and entrainment of subsurface water into the mixed layer

The horizontal domain of OGCM is 120° E–76° W, 30° S–30° N, with the resolution about 1° in the central basin and being gradually enhanced to 0.4° in the west and east boundary regions in the zonal direction, and about 0.3°–0.6° between 30° S and 30° N and being gradually increased to 2° in the north and south boundaries. Temperature, salinity and other variables are all restored to World Ocean Atlas 1998 (WOA98) climatology at sponge boundaries (within 10° of the north and south boundaries). The penetration depth (H$_p$) of sunlight into the upper ocean is prescribed to be seasonally dependent climatology determined by historical ocean color data (Zhang 2015).

The statistical atmospheric anomaly model consists of an interannual anomaly model and tropical instability wave (TIW)-induced perturbation model for wind stress, and a FWF anomaly model. Heat Flux is calculated by the advection atmospheric mixed layer model (Seager et al. 1995). The full field of wind stress (τ) can be written as $\tau = \tau_{clim} + \tau_{inter} + \tau_{TIW}$, in which τ_{clim} is seasonally varying climatological wind stress prescribed from observation, τ_{inter} is interannual wind stress anomaly, and τ_{TIW} is wind stress perturbation induced by TIW. τ_{inter} is empirically related to interannual SST vatiation (denoted as SST$_{inter}$), written as $\tau_{inter} = \alpha_{inter} \times F_\tau$ (SST$_{inter}$),

in which F$_\tau$ is the relationship between interannual anomalies of τ and SST which can be derived using SVD method from historical data; seasonally dependent model for τ_{inter} is adopted (Zhang and Zebiak 2004). A scalar parameter, α_{inter}, is introduced to represent the intensity of interannual wind forcing; α_{inter} is taken as 1.18 ($\alpha_{inter} = 1.18$). τ_{TIW} is wind stress perturbation induced by TIW, written as $\tau_{TIW} = \alpha_{TIW} \times F_{TIW}$ (SST$_{TIW}$), a statistical model which is constructed based on SVD analysis using 12° zonal smooth filtered daily Quick Scatterometer (QuikSCAT) wind stress (τ_{TIW}) and Tropical Rainfall Measuring Mission (TRMM) Microwave Imager (TMI) SST (SST$_{TIW}$) data covering the eastern Pacific (10° S–10° N, 180°–90° W) (Zhang and Busalacchi 2009b). F$_{TIW}$ is the relationship between the TIW-scale wind stress (τ_{TIW}) and SST (SST$_{TIW}$); α_{TIW} is introduced to represent the intensity of TIW wind forcing. Here, α_{TIW} is taken as 3.0 ($\alpha_{TIW} = 3.0$).

In the tropical Pacific, FWF, here defined as precipitation (P) minus evaporation (E), exhibits strong interannual variability, which is closely related to ENSO. The full field of FWF can be decomposed into seasonal climatological part ((P − E)$_{clim}$) and interannual anomaly part ((P − E)$_{inter}$), written as FWF = (P − E)$_{clim}$ + (P − E)$_{inter}$. The interannual

variation of FWF is calculated by a statistical model based on SVD analysis using historical FWF and SST anomaly data, written as $(P − E)_{inter} = \alpha_{FWF} \times F_{FWF}(SST_{inter})$. A parameter, α_{FWF}, is introduced to represent the coupled intensity between FWF and SST. Here, α_{FWF} is taken as 1.5 ($\alpha_{FWF} = 1.5$). In order to take into consideration of seasonal variations, 12 sub-models for $(P − E)_{inter}$ are constructed for each calendar month (Zhang and Busalacchi 2009a).

Two pathways exist through which FWF can affect the ocean: one through SSS and the other through buoyance flux (Q_B). The first pathway of the FWF effect on SSS acts as a source term to affect SSS as described by the conservation equation of salt in the ocean model. The variation of SSS plays an important role in determining the oceanic density, which thereby influences the upper ocean stability and vertical mixing. The second pathway of the FWF effect on Q_B acts as a forcing term in the bulk mixed layer model along with heat flux and wind to explicitly determine variation of MLD, which affects the entrainment of subsurface water into the mixed layer and vertical mixing.

In the Kraus−Turner (KT) ML model, the entrainment rate at the base of the ML is determined by a bulk turbulent energy equation as follows,

$$\frac{\partial h_m}{\partial t} \Delta b h_m = 2m_0 u_*^3 + h_m B_0 - (1 - n_0)h_m$$
$$\left[B_0 + |B_0| \right]/2 + J_0 \left[h_m - 2h_p + (h_m + 2h_p)e^{-\frac{h_m}{h_p}} \right]$$

in which h_m is the ML depth; B is buoyancy flux and B_0 is buoyancy flux at the sea surface, including the contribution of FWF; h_p is the penetration depth of solar radiation in the upper ocean; m_0 and n_0 are empirical coefficients; the meanings of other fields can be found in Chen et al. (1994). As expressed, the first term on the right side, $2m_0 u_*^3$, mainly represents the turbulent kinetic energy (TKE) input by wind stirring, acting to deepen the mixed layer; the second term is the rate of potential energy inserted into the mixed layer due to surface buoyancy (B_0) effects which include the contribution of heat flux and FWF at the sea surface; the third term is a dissipative term to reduce term B_0 when convective overturn is occurring ($B_0 > 0$); and the fourth term is the effects of penetrating radiation on TKE within the mixed layer. The KT ML model represents an integrated form of the TKE over the mixed layer and can be used to explicitly predict the depth of ML. It assumes that the integration of TKE produced by wind stirring and unstable convection by B_0 over the mixed layer must balance with the energy needed to entrain the water below. As part of B_0, thus, FWF is a factor that directly determines the MLD and its variation, providing a pathway through which interannual FWF anomalies can directly affect h_m and the ocean state.

Q_B at the ocean surface can be expressed as

$$Q_B = \alpha \cdot HF/(\rho \cdot C_p) + \beta \cdot S_0 \cdot FWF = Q_T + Q_S \quad (1)$$

where HF and FWF are the net heat flux and freshwater flux at the sea surface, respectively; ρ is the density of seawater, C_p is the heat capacity and S_0 is the reference surface salinity; α and β are the thermal and haline coefficients of expansion, respectively. As expressed, Q_B is the sum of the heat flux (Q_T) and freshwater flux (Q_S). The principle here is that positive buoyancy flux (a positive anomaly) represents an influx into the sea surface, so that the surface layer becomes more buoyant with reduced buoyant force, which acts to reduce the MLD and mixing (Zhang and Bussalachi 2009a). The ocean can have a response to the perturbation of Q_B through a gravitational adjustment. Because ML formulation is explicitly related to the wind stirring and the net buoyancy flux in the tropical ocean, FWF, as part of Q_B, has a direct impact on MLD, which in turn affects the upper ocean mixing and the entrainment of subsurface water into the mixed layer (Chen et al. 1994). Note that, the mixed layer dynamics represented in the layer ocean models (the direct effects of FWF on shoaling or deepening of the ML) has been considered as one of the main missing processes in the level models, in which the pathway of FWF effect on Q_B does not exist explicitly.

The coupling integration process of the HCM is as follows: for each time step, the OGCM is integrated to update the SST fields, which are averaged to obtain daily mean SST. The SST climatology (SST_{clim}) field is preprocessed using the OGCM forced by observed τ_{clim}, and then the daily SST anomaly can be calculated. Heat flux is calculated from the AML model using the OGCM SST field. For each day, the interannual anomaly fields (τ_{inter} and $(P-E)_{inter}$) and TIW field (τ_{TIW}) are calculated using their corresponding statistical models, and then are added to their prescribed climatological fields (τ_{clim} and $(P-E)_{clim}$) to force the OGCM. τ_{clim} and P_{clim} are prescribed from observation; E_{clim} is calculated from the AML model using simulated SST_{clim} field. The heat flux and FWF are used to calculate Q_B, which is then used to additionally force the bulk mixed layer model in our layer ocean model.

2.2 Experimental design

Experiments designed to examine differently represented FWF effects on ENSO are shown in Table 1. There exist two influence pathways induced by interannual FWF variability in modulating ENSO in the ocean: one through SSS and the other through Q_B. Correspondingly, four experiments are designed as follows: Expt. 1 is denoted as FWF(S_{inter}, B_{inter}), in which interannual FWF effects on the ocean are represented collectively both by SSS and Q_B; Expt. 2 is denoted as FWF(S_{inter}, B_{clim}), in which only interannual FWF effect on SSS is represented, whereas that on Q_B is

purposely excluded and a seasonally varying FWF climatology is prescribed for use in calculating Q_B; Expt. 3 is denoted as FWF(S_{clim}, B_{inter}), in which only interannual FWF effect on Q_B is represented, whereas that on SSS is purposely excluded and a seasonally varying FWF climatology is prescribed for use in accounting for its effect on SSS; Expt. 4 is denoted as FWF(S_{clim}, B_{clim}), in which interannual FWF effect is not taken into account in the HCM and FWF is prescribed as seasonally varying climatology. These experiments can be compared with each other to clearly and quantitatively illustrate modulations of differently represented FWF effects on ENSO, and separately demonstrate model biases associated with differently represented FWF in the HCM. All the experiments are integrated for 100 years from the same initial conditions that are chosen arbitrarily from a sustained coupled integration (denoted as year 1), and the last 80-year (from year 21 to 100) simulations are used for analyzing the roles of interannual FWF variability in modulating ENSO through its effects either on SSS or Q_B, respectively.

3 Positive feedback on ENSO induced by interannually varying FWF

In the tropical Pacific, interannual variations of FWF and its associated ocean salinity anomalies are closely related with ENSO (Qu et al. 2014; Zhang et al. 2012). FWF is

Table 1 Experiments designed to examine the role played by interannual FWF variability in modulating ENSO through its effects on either SSS or buoyancy flux (Q_B), respectively; correspondingly, there exist two influence pathways induced by interannual FWF variability on the ocean: one through SSS and the other through Q_B

Experiments	Experiments in which SSS and Q_B are affected by interannually varying and climatological FWF effects		Denoted names
	SSS	Buoyancy flux	
Expt. 1	FWF(S_{inter})	FWF(B_{inter})	FWF(S_{inter}, B_{inter})
Expt. 2	FWF(S_{inter})	FWF(B_{clim})	FWF(S_{inter}, B_{clim})
Expt. 3	FWF(S_{clim})	FWF(B_{inter})	FWF(S_{clim}, B_{inter})
Expt. 4	FWF(S_{clim})	FWF(B_{clim})	FWF(S_{clim}, B_{clim})

FWF(S_{inter}, B_{inter}) is denoted as a run, in which interannual FWF effects on SST and Q_B are both represented. FWF(S_{inter}, B_{clim}) is denoted as a run, in which only interannual FWF effect on SSS is represented, whereas that on Q_B is purposely excluded and a seasonally varying FWF climatology is prescribed for use in calculating Q_B in the bulk mixed model. FWF(S_{clim}, B_{inter}) is denoted as a run, in which only interannual FWF effect on Q_B is represented, whereas that on SSS is purposely excluded and a seasonally varying FWF climatology is prescribed for use in accounting for its effect on SSS. FWF(S_{clim}, B_{clim}) is denoted as a run, in which interannual FWF effects are not taken into account in the HCM (i. e., FWF is prescribed as seasonally varying climatology)

an important atmospheric forcing to the ocean, which can affect ENSO; at the same time, FWF and its associated SSS are affected by ENSO (Zhu et al. 2014). The HCM with represented interannual FWF effects both on SSS and Q_B can well depict the tropical Pacific interannual variability associated with ENSO.

Consider an example segment of interannual anomalies of SST, FWF and SSS in FWF(S_{inter}, B_{inter}) during the last 20-year simulation. Long-term integrations indicate that the HCM can produce reasonable and sustainable ENSO periodicity and amplitude (Fig. 2a). For instance, the interannual variations of FWF and SSS anomalies are accompanied with the SST anomalies. When large warm SST anomalies occur in the central and eastern tropical Pacific, the positive FWF anomalies appear to the west, along with negative SSS anomalies there. Similarly, cold SST anomalies in the east are accompanied with negative FWF anomalies and positive SSS anomalies (Fig. 2b, c) in the western equatorial Pacific.

FWF exhibits the strongest interannual variability in the western-central equatorial Pacific near the dateline. Interannual FWF variability has a positive feedback on ENSO, which has a significant enhancing impact on ENSO amplitude. The interannual FWF effects can be illustrated by comparing simulations FWF(S_{inter}, B_{inter}) with those in FWF(S_{clim}, B_{clim}). Maps of the averaged anomalies for some related ocean variables in December–January–February (DJF) of the composite El Niño events simulated in FWF(S_{inter}, B_{inter}) and FWF(S_{clim}, B_{clim}) are shown in Fig. 3. During El Niño peak stage, the maximum warm SST anomalies are located in the central and eastern tropical Pacific (Fig. 3a), accompanied by positive FWF anomalies in the west. The freshening of the upper ocean leads to negative SSS anomalies in the central Pacific (Fig. 3b). As a result, the upper ocean becomes fresher and thus more stable, suppressing the vertical mixing and entrainment of cold water underneath, enhancing the positive SST anomalies in situ. Meanwhile, the positive FWF anomalies also induce negative Q_B anomalies in the central equatorial Pacific (Fig. 3c), which further leads to a shoaling of the ML in the western tropical Pacific; a clear see-saw pattern exists in the zonal direction, with the mixed layer being shallower in the western and central Pacific, but deeper in the east (Fig. 3d). Thus, the changes in MLD induced by the positive FWF anomaly are of the same sign with those produced by Bjerknes feedback (Bjerknes 1969). These accordingly inhibit the vertical mixing and the entrainment of subsurface cold water into the mixed layer, thus making SST warmer in the central and eastern Pacific (Fig. 3a). Larger interannual anomalies of these fields are seen in FWF(S_{inter}, B_{inter}) (the left column of Fig. 3) than those in FWF(S_{clim}, B_{clim}) (the right column of Fig. 3). That is, the interannual FWF effects tend to enhance the related ocean processes. As a result, these oceanic processes serve as a
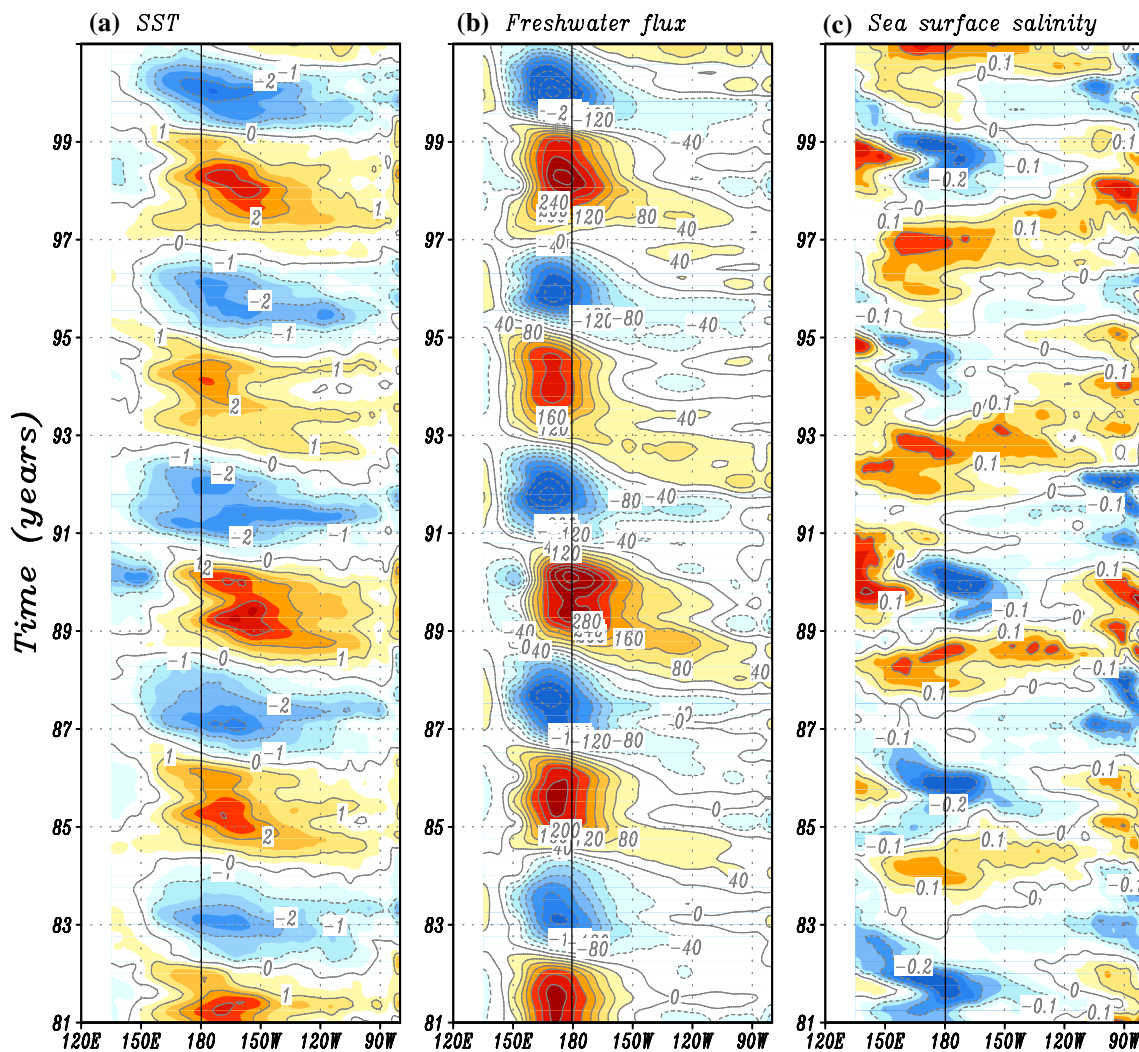
Fig. 2 Interannual variations along the equator for **a** SST, **b** FWF, **c** SSS anomalies simulated in FWF(S_{inter}, B_{inter}). The experiment is integrated for 100-year and the last 20-year (from model year 81 to 100) simulation is shown. The contour interval is 1.0 °C in **a**, 40 mm month^{-1} in **b** and 0.1 psu in **c**

positive feedback on ENSO that is induced by interannual FWF variability.

From time series of the Niño3.4 SST anomalies in these experiments (Fig. 4), it is evident that sustained ENSO cycles are produced, whereas the amplitudes of the Niño3.4 SST anomalies are different from each other due to the modulation of the differently represented interannual FWF forcing. For example, the Niño3.4 SST anomalies in FWF(S_{inter}, B_{inter}) are substantially larger compared with those in the FWF(S_{clim}, B_{clim}). This means that the represented interannual FWF effects collectively through the SSS and Q_B pathways can act as a positive feedback on ENSO as indicated in FWF(S_{inter}, B_{inter}) (Fig. 5).

Coherent patterns and interrelationships are seen among interannual anomalies of SST, SSS, Q_B and MLD fields

(Figs. 6, 7, 8, 9). The simulated SST anomalies exhibit large interannual variations with a nonlocal positive correlation with FWF during ENSO cycles. In FWF(S_{inter}, B_{inter}), in which the interannual FWF effects both on SSS and Q_B are represented, there exists a pronounced ENSO cycle with the amplitude about more than 2.5 °C in almost all ENSO events, sometimes even larger than 3 °C during ENSO peak stage (Fig. 6a). In FWF(S_{clim}, B_{clim}), ENSO intensity is obviously underestimated, with the amplitude only about 1 °C (Fig. 6b).

To illustrate the modulation of interannual FWF variability on SST, we then separately check the variations of SSS and Q_B fields, which are two fields directly affected by FWF forcing. The anomalous FWF induced by ENSO is expected to have a direct effect on SSS. As shown, the

Anomalies averaged in DJF
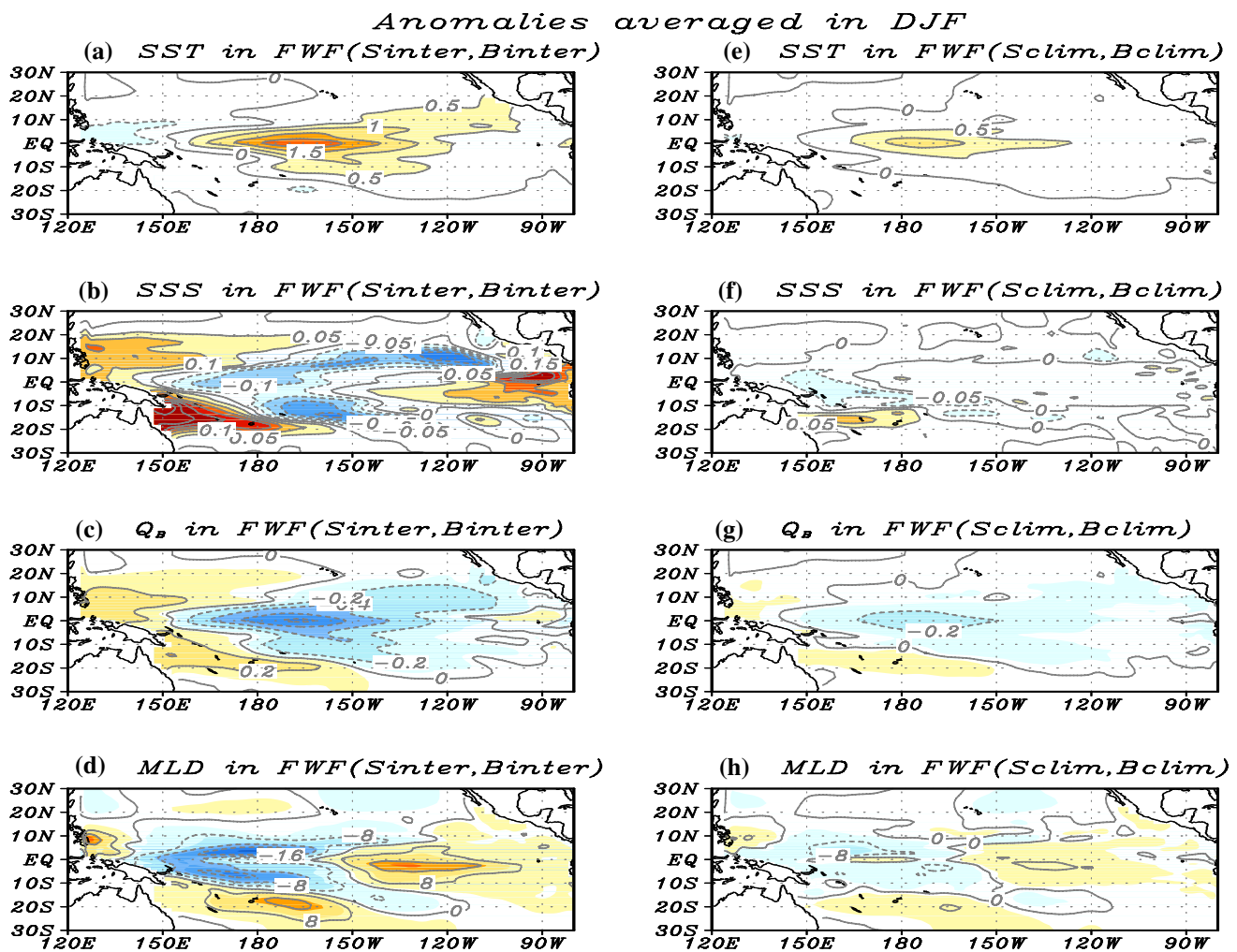
Fig. 3 Maps of averaged anomalies in DJF (December–January–February) for the composite El Niño events simulated in FWF(S_{inter}, B_{inter}) (left panel) and FWF(S_{clim}, B_{clim}) (right panel): **a, e** SST, **b, f** SSS, **c, g** Q_B, and **d, h** MLD. The contour interval is 0.5 °C for SST, 0.05 psu for SSS, 0.2×10^{-6} kg s^{-1} m^{-2} for Q_B, and 8 m for MLD

largest variability center of FWF is located in the western-central basin near the dateline, where SSS variability is also large. The direct effect of positive (negative) FWF anomalies is to reduce (increase) SSS in the western and central Pacific (Fig. 7) and Q_B. Another pathway is through the effect on Q_B. For example, Q_B anomaly in model year 23 simulated from FWF(S_{inter}, B_{inter}) is negative in the western and central Pacific (Fig. 8a); at the same time, Q_T anomaly is negative (the opposite sign to SST anomaly in Fig. 6a) and Q_S anomaly is positive (the same sign with FWF anomaly in Fig. 5a). As shown in Eq. (1), buoyance flux consists of heat flux and freshwater flux; Q_S has direct impacts on Q_B, which is also simultaneously affected by Q_T (Zhang and Busalacchi 2009b). Here, the sign of Q_B anomaly (negative) is the same as the Q_T anomaly, but opposite to the Q_S anomaly (positive). Hence, the Q_S variability induced by interannual FWF variability has out-of-phase relationship with

Q_T, acting to reduce the amplitude of Q_B variability during ENSO cycles. In FWF(S_{inter}, B_{inter}), the maximum amplitude of Q_B anomaly is greater than 1.0×10^{-6} kg s^{-1} m^{-2}, whereas in FWF(S_{clim}, B_{clim}), it is only about 0.2×10^{-6} kg s^{-1} m^{-2} during most ENSO peak stages.

In the bulk mixed layer model, MLD is associated with the ratio of wind generation of turbulent kinetic energy to the net positive buoyancy flux, so the decreased (increased) Q_B anomalies induced by positive (negative) FWF anomalies leads to a decrease (an increase) in MLD in the western and central equatorial Pacific (Figs. 5, 8, 9). The MLD variations further affect the vertical mixing and entrainment at the base of mixed layer. The interannual MLD variations along the equator obviously show a seesaw pattern in the zonal direction (Fig. 9), which is the same as that seen in Fig. 3d. This tends to flatten (deepen) the mixed layer during El Niño (La Niña) phase.

Fig. 4 Time series of the Niño 3.4 SST anomalies (units: °C) in FWF(S_{inter}, B_{inter}) (black), FWF(S_{clim}, B_{clim}) (blue), FWF(S_{inter}, B_{clim}) (red) and FWF(S_{clim}, B_{inter}) (yellow) during the last 80-year simulation
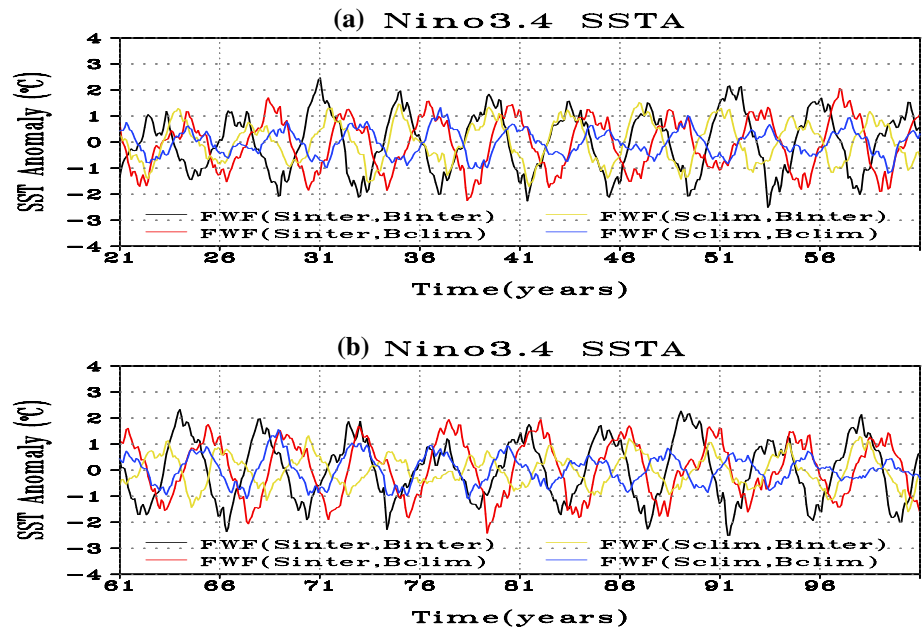

Here, the standard deviation is used as a measure to quantify the effects on some specific ocean variables. To illustrate the magnitude of interannual variability for ENSO events, the standard deviations for SST anomalies along the equator calculated from the last 80-year model simulation in FWF(S_{inter}, B_{inter}) and FWF(S_{clim}, B_{clim}) are shown in Fig. 10. As expected, the standard deviation of SST anomalies in FWF(S_{inter}, B_{inter}) is large with the maximum value about 2 °C located around 170° W, whereas that in FWF(S_{clim}, B_{clim}) is small with the maximum value only about 0.9 °C.

Many previous studies have found strong dominant influence of wind forcing, including high-frequency westerly wind bursts, on ENSO generation and development in the tropical Pacific. Note that according to Fig. 10, the ENSO strength in FWF(S_{clim}, B_{clim}) becomes much weaker when interannual FWF effect is disabled in FWF(S_{inter}, B_{inter}). This does not mean that the wind contribution is of secondary importance compared to freshwater flux forcing. In fact, the interannual FWF forcing-induced wind effect (indirect) is also important in the model simulations. That is, interannual FWF forcing actually induces a direct effect and indirect effect. The former is realized through SSS and Q_B, whereas the latter is manifested as coupled ocean-interactions. The interaction loop involves the direct effects of interannal FWF anomalies on SSS and Q_B, which cause changes in the ocean dynamical processes that affect SST, which induces a response of wind stress, which in turn affects the oceans, producing coupled ocean-interactions. So, the results in FWF(S_{clim}, B_{clim}) and FWF(S_{inter}, B_{inter}) indicate a reduction role of the FWF forcing through a positive air-sea feedback,

showing that excluding the interannual FWF forcing at the air-sea interface reduces the ENSO amplitudes in FWF(S_{clim}, B_{clim}). Also note that large-scale wind stress anomalies in the HCM are calculated from a statistical feedback model constructed from historical data; high-frequency wind forcing effects such as westerly wind bursts are not taken into account. So, the HCM can underestimate the influence of wind forcing.

Notice that the HCM we used in this modeling study has obvious discrepancies compared with corresponding observations. For example, one bias in the HCM simulations is that in terms of SST variability, the El Niño events presented in Fig. 2a are all central Pacific (CP) type with the maximum SST warming around the dateline; in nature, there are two types of El Niño: eastern Pacific (EP) and CP El Niño. In addition, the simulated ENSO cycles in our HCM are the way too regular. These discrepancies can be partly attributed to the fact that statistical models for atmospheric interannual anomalies of wind stress and FWF are used, so precluding the effects of stochastic forcing on the ocean simulations. So, the biases seen in the simplified HCM simulations may modify the conclusions qualitatively. These issues need to be analyzed in the future. Nevertheless, even though the simulated ENSO events are much idealistic compared with corresponding observations, the HCM can well capture the ENSO related cycles for representing the basic ENSO dynamics, including FWF effects. Also, the simplified HCM can be effectively and efficiently used to conduct sensitivity experiments in the coupled system to further understand ENSO modulations induced by FWF forcing.

FWF anomalies along the equator
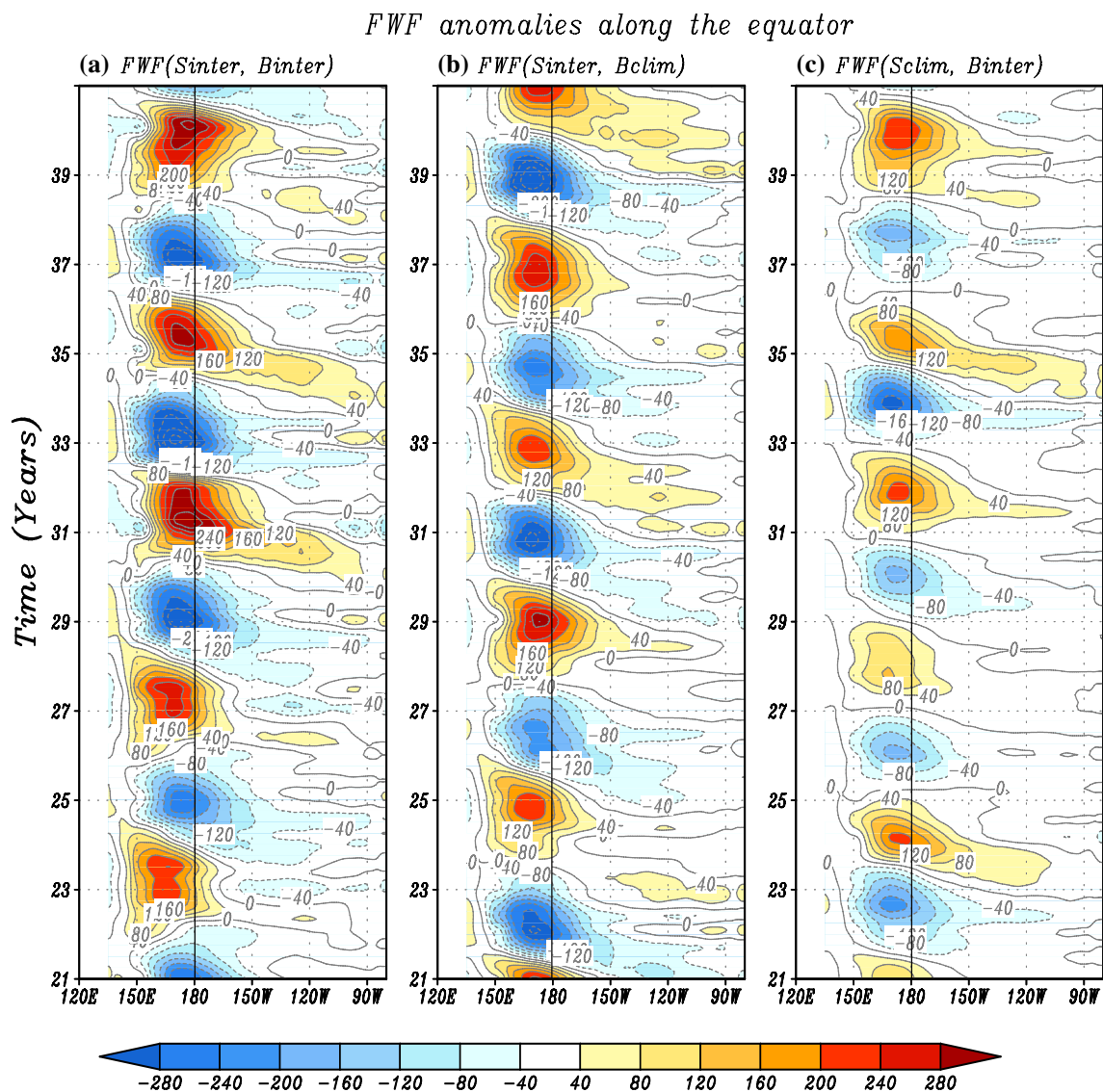
Fig. 5 Interannual variations along the equator for FWF anomalies during the model 21–40 year simulation in **a** FWF(S_{inter}, B_{inter}), **b** FWF(S_{inter}, B_{clim}), and **c** FWF(S_{clim}, B_{inter}). The contour interval is 40 mm month^{-1}

4 The FWF effects on ENSO through individual pathway

As illustrated in Fig. 1, two influence pathways exist by which interannual FWF variability can affect the ocean: one through SSS and the other through Q_B. The sensitivity experiments using the HCM descibed in Sect. 2 are conducted to quantify modulations of the differently represented FWF effects on ENSO. In this section, the interannual FWF effects on ENSO through the SSS or Q_B pathways are individually illustrated and quantified.

4.1 The SSS influence pathway

When only considering the interannual FWF effect through SSS pathway, the simulated interannual FWF amplitude in FWF(S_{inter}, B_{clim}) is about 200 mm month^{-1} during most ENSO stage (Fig. 5b), which is slightly weaker than that in FWF(S_{inter}, B_{inter}), which exhibits the maximum anomaly that exceeds 280 mm month^{-1} during almost all ENSO peak stages (Fig. 5a). When interannual FWF variability effect is represented only through the SSS pathway in FWF(S_{inter}, B_{clim}), ENSO amplitude (with the amplitude about 2 °C in Fig. 6c) is stronger than that in FWF(S_{clim}, B_{clim}) but is weaker than that in (S_{inter}, B_{inter}).

The strength of interannual SSS variability in FWF(S_{inter}, B_{clim}) (Fig. 7c) is almost the same as that in FWF(S_{inter},
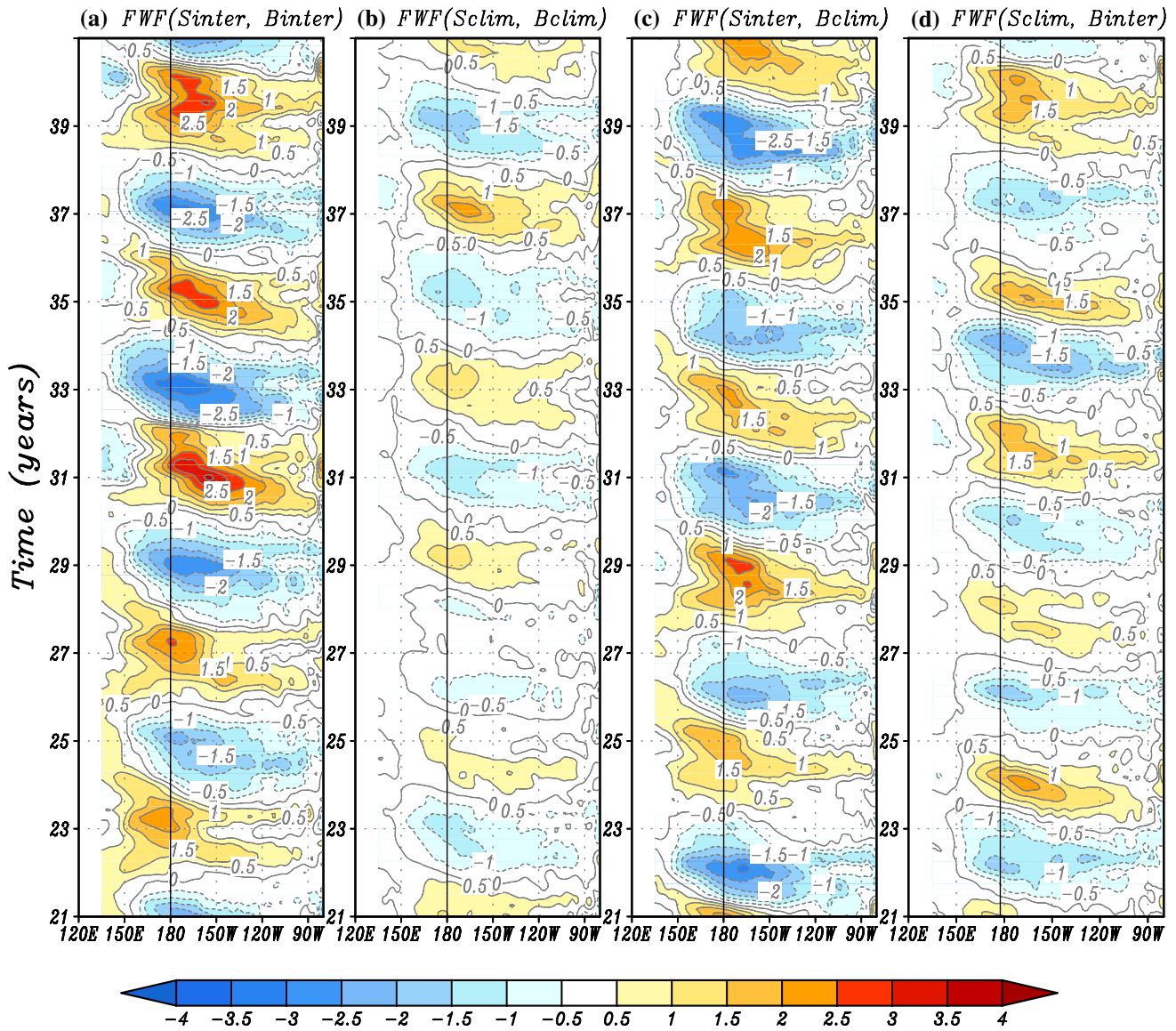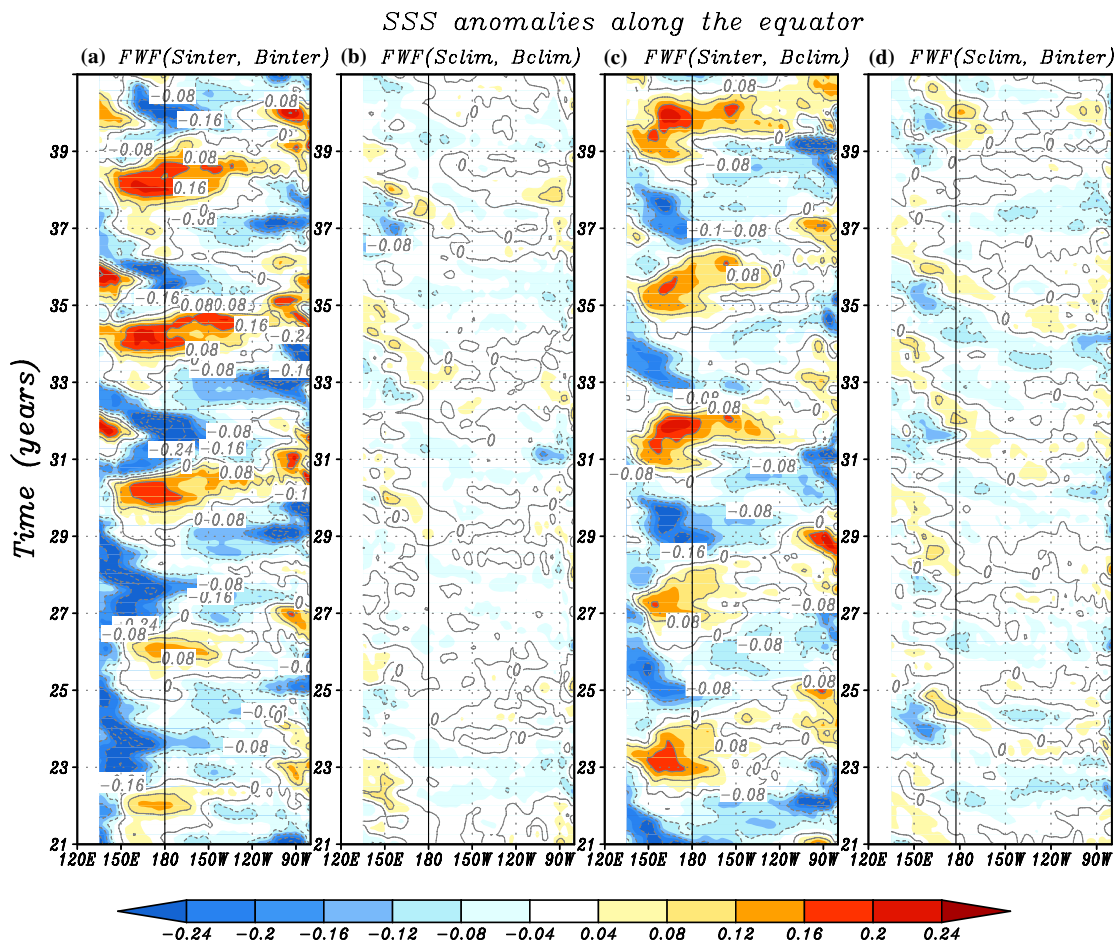
SST anomalies along the equator

Fig. 6 Interannual variations along the equator for SST anomalies during the model 21–40 year simulation in **a** FWF(S_{inter}, B_{inter}), **b** FWF(S_{clim}, B_{clim}), **c** FWF(S_{inter}, B_{clim}), and **d** FWF(S_{clim}, B_{inter}). The contour interval is 0.5 °C

B_{inter}) (Fig. 7a), with the amplitude about 0.16 psu, which is much stronger than that in FWF(S_{clim}, B_{clim}) as indicated in Fig. 7b. It illustrates that the SSS pathway is a major pathway by which interannual FWF variability can strongly impact interannual SSS variability. Also, the amplitude of Q_B anomaly is about 0.6×10^{-6} kg s^{-1} m^{-2} during most ENSO peak stages in FWF(S_{inter}, B_{clim}). The maximum MLD anomaly value of the zonal seesaw pattern in FWF(S_{inter}, B_{clim}) is about 16 m (sometimes it can exceed 24 m as indicated in Fig. 8c), but it is weaker than that in FWF(S_{inter}, B_{inter}), whose maximum is 32 m. The ENSO related interannual

FWF variability tends to reinforce the MLD seesaw pattern, which contributes to a positive effect on SST.

Changes in these oceanic processes in turn affect SST anomalies, which are consistent with SST variations shown in Fig. 6. From time series of the Niño3.4 SST anomalies (Fig. 4), it is seen that the Niño3.4 SST anomaly in FWF(S_{inter}, B_{clim}) is smaller than that in FWF(S_{inter}, B_{inter}). This suggests that when the interannual FWF effect is represented through the SSS pathway but not through the Q_B pathway (such as in level ocean models), the interannual FWF effects may be underestimated compared with those in

SSS anomalies along the equator

Fig. 7 Interannual variations along the equator for SSS anomalies during the model 21–40 year simulation in **a** FWF(S_{inter}, B_{inter}), **b** FWF(S_{clim}, B_{clim}), **c** FWF(S_{inter}, B_{clim}), and **d** FWF(S_{clim}, B_{inter}). The contour interval is 0.08 psu

which both the SSS and Q_B pathways are represented (such as layer models).

After validating the modulation on interannual variations, the changes in ENSO amplitude induced by interannual FWF variability through the SSS pathway is quantitatively illustrated. The standard deviations for SST anomalies along the equator calculated from the last 80-year model simulation in the four experiments are shown in Fig. 10. The standard deviation of SST anomalies in FWF(S_{inter}, B_{clim}) is almost the same as that in FWF(S_{inter}, B_{inter}). It indicates that the interannual FWF variability contributes to a positive feedback on ENSO because the interannual variability induced by interannually varying FWF is substantially stronger than in FWF(S_{clim}, B_{clim}). Additionally, these sensitivity experiments confirm a major role played in FWF positive feedback by interannual FWF effect represented through SSS pathway. Comparisons of FWF standard deviations indicate that the FWF variability is centered

in the central tropical Pacific, with the maximum values being 240 mm month^{-1} in FWF(S_{inter}, B_{inter}) (Fig. 11a) and 210 mm month^{-1} in FWF(S_{inter}, B_{clim}) (Fig. 11b), respectively.

Specifically, the spatial patterns for standard deviations of the related ocean variables are illustrated below. The maps for standard deviations of SST anomalies shown in Fig. 12 indicate that these experiments exhibit the maximum SST variations that are centered in the central equatorial Pacific. When only interannual FWF effect is represented through SSS pathway, the maximum variation value is about 1.6 °C (Fig. 12c). When interannual FWF effects through SSS and Q_B pathways are both represented, the maximum variation value is about 1.8 °C (Fig. 12a), which is much larger than that without considering interannual FWF effect, which is only 0.8 °C (Fig. 12b). That means the interannual FWF variability serves as a positive feedback on SST variation, and the differently represented FWF forcing can change the strength of feedback.
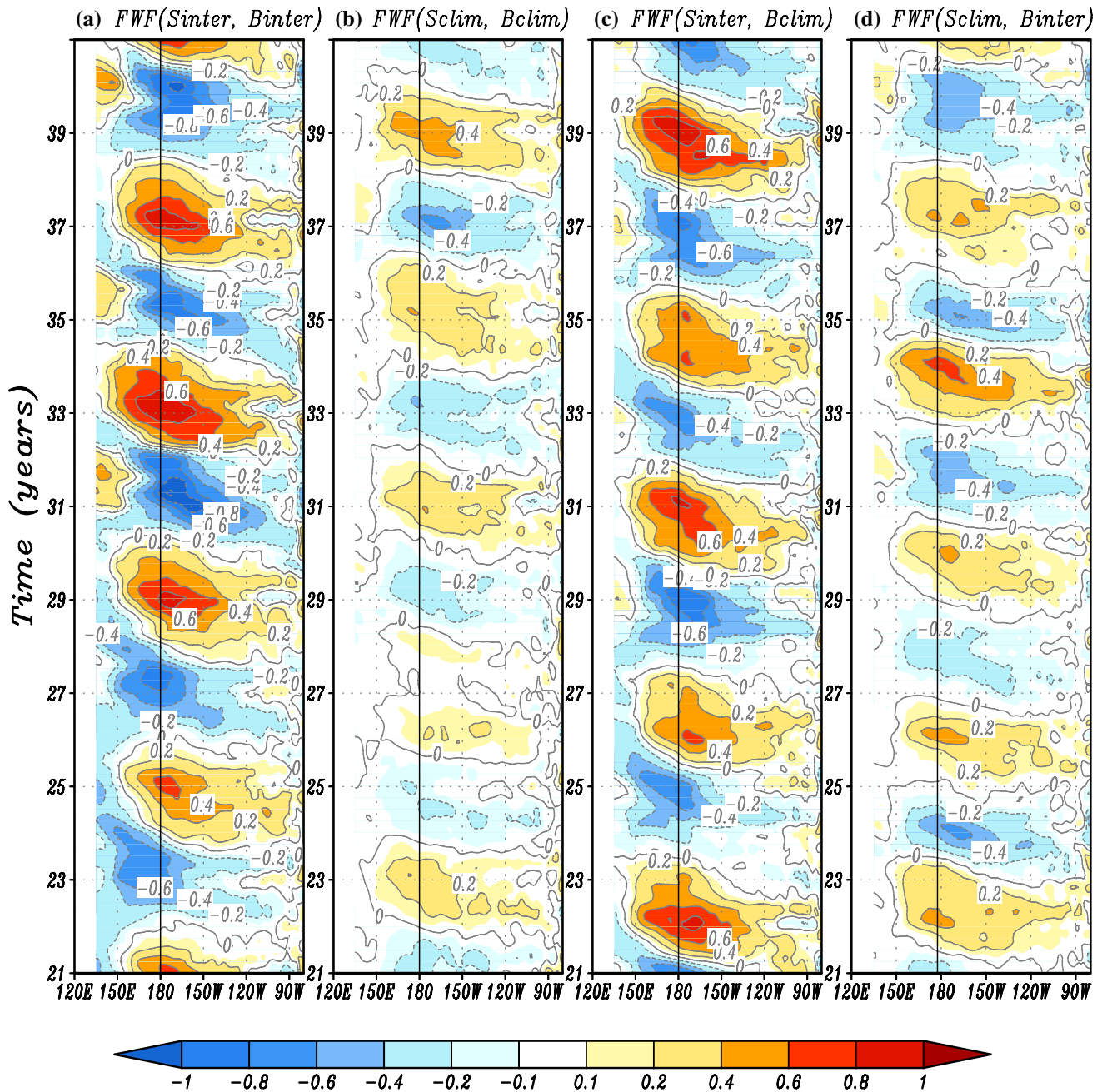
Fig. 8 Interannual variations along the equator for Q_B anomalies during the model 21–40 year simulation in **a** FWF(S_{inter}, B_{inter}), **b** FWF(S_{clim}, B_{clim}), **c** FWF(S_{inter}, B_{clim}), and **d** FWF(S_{clim}, B_{inter}). The contour interval is 0.2×10^{-6} kg s^{-1} m^{-2}

It is clear that if only considering interannual FWF effect on the ocean through SSS pathway, it underestimates the strength of SST variation compared with simulations in which interannual FWF effects are considered through affecting SSS and Q_B pathways.

The maximum SSS variations are centered in the subtropical Pacific (10° S–20° S, 10° N–20° N). When only considering interannual FWF effects through SSS pathway, the maximum value is about 0.21 psu (Fig. 13c), which is almost the same as that when interannual FWF effects are considered through SSS and Q_B pathways (Fig. 13a). The values in FWF(S_{inter}, B_{inter}) and FWF(S_{inter}, B_{clim}) are much larger than those in FWF(S_{clim}, B_{clim}). This is because FWF can have a direct effect on SSS, serving as a source term in the salinity equation. Maps of standard deviations for Q_B anomalies are shown in Fig. 14. In FWF(S_{inter}, B_{clim}), the
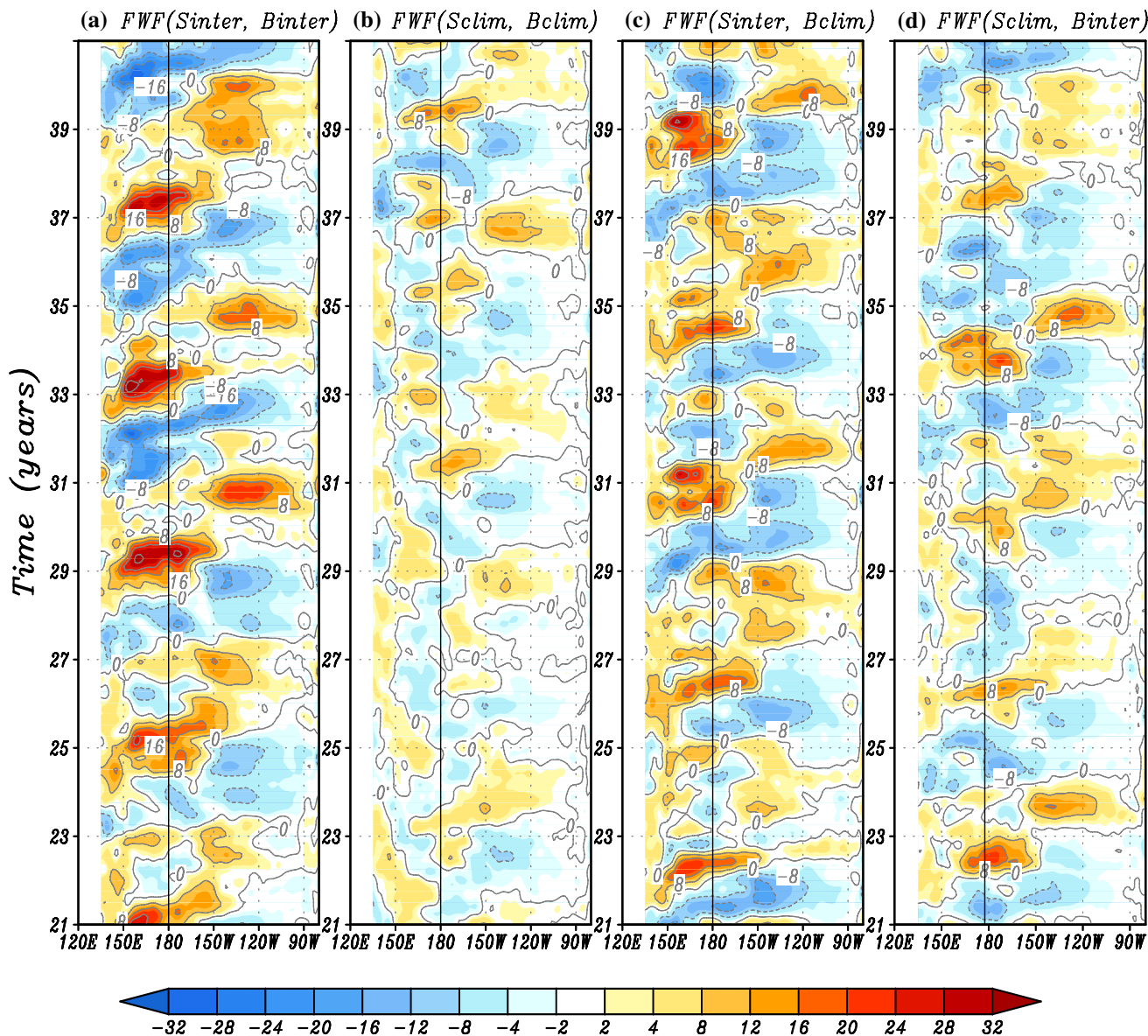
Fig. 9 Interannual variations along the equator for MLD anomalies during the model 21–40 year simulation in **a** FWF(S_{inter}, B_{inter}), **b** FWF(S_{clim}, B_{clim}), **c** FWF(S_{inter}, B_{clim}), and **d** FWF(S_{clim}, B_{inter}). The contour interval is 8 m

maximum value for standard deviation of Q_B anomalies is about 0.5×10^{-6} kg s^{-1} m^{-2} (Fig. 14c), with the maximum variability being centered in the central tropical Pacific. In FWF(S_{inter}, B_{inter}), the maximum value for standard deviation of Q_B anomalies is about 0.6×10^{-6} kg s^{-1} m^{-2} (Fig. 14a), whereas it is only about 0.2×10^{-6} kg s^{-1} m^{-2} in FWF(S_{clim}, B_{clim}) (Fig. 14b).

The variations of SSS and Q_B further affect the upper ocean stability, vertical mixing and entrainment of subsurface water into mixed layer. Thus, the maps for standard deviations of MLD anomalies are checked (Fig. 15). The maximum areas of MLD variability are centered in

the western and central Pacific. When interannual FWF effects through SSS and Q_B pathways are both represented, the maximum value for standard deviation of MLD is about 21 m, being located both in the north and south subtropical Pacific (Fig. 15a), which is much larger than that without considering interannual FWF effect (only 9 m in FWF(S_{clim}, B_{clim}); Fig. 15b). When interannual FWF effect through SSS pathway is only represented, the maximum value for standard deviation of MLD is about 18 m, which is located in the south subtropical Pacific (Fig. 15c). The different amplitudes of MLD variability induced by differently represented interannual FWF effects in turn

Fig. 10 Standard deviations of SST anomalies (°C) along the equator calculated from the last 80-year simulation in FWF(S_{inter}, B_{inter}) (black), FWF(S_{clim}, B_{clim}) (blue), FWF(S_{inter}, B_{clim}) (red) and FWF(S_{clim}, B_{inter}) (yellow)
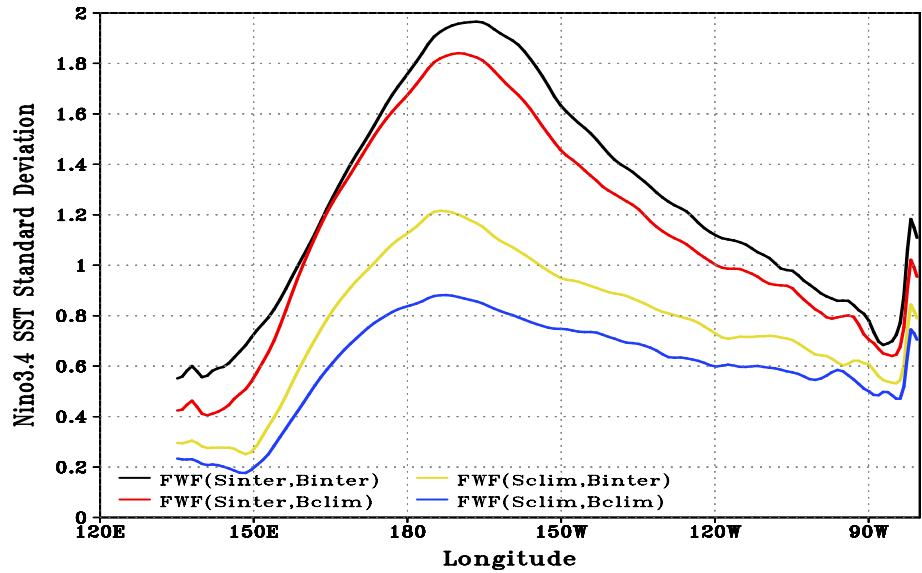
Fig. 11 Maps for standard deviations of FWF anomalies calculated from the last 80-year simulation in **a** FWF(S_{inter}, B_{inter}), **b** FWF(S_{inter}, B_{clim}), and **c** FWF(S_{clim}, B_{inter}). The contour interval is 30 mm month^{-1}
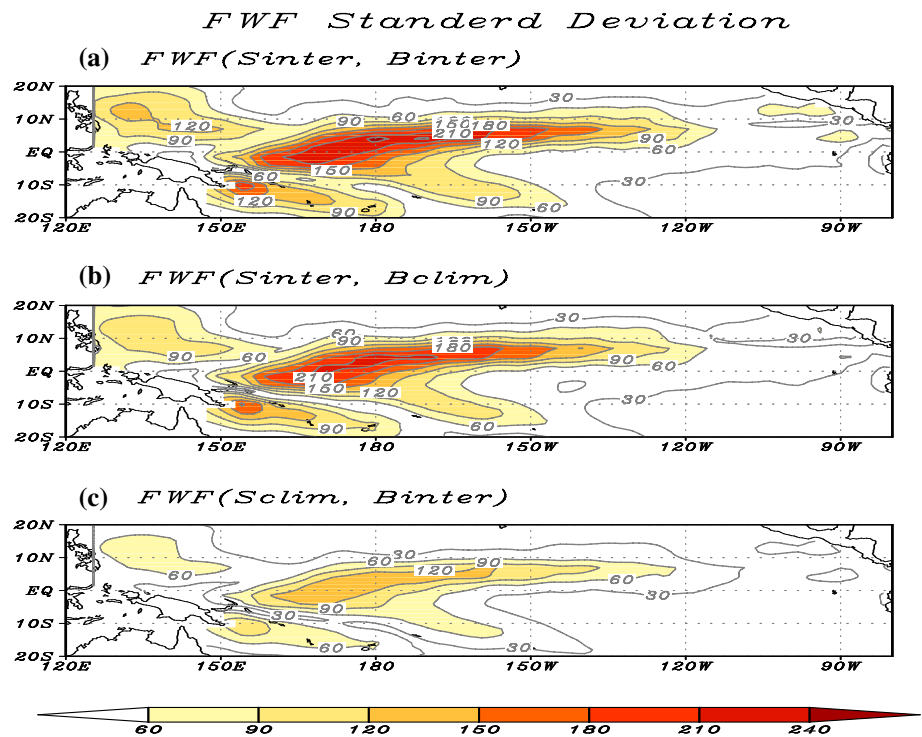
correspond to different effects on SST, which is consistent with the maps for standard deviations of SST anomalies shown in Fig. 12.

In order to quantify the changes in ENSO amplitude by the differently represented FWF effect, we calculate the percentage changes in standard deviations of key ocean variables in the Niño 3.4 area. That is, the percentage of the difference between FWF(S_{inter}, B_{clim}) and FWF(S_{clim}, B_{clim}) relative to the difference between FWF(S_{inter}, B_{inter}) and FWF(S_{clim}, B_{clim}) is calculated. This value represents

the change in amplitude induced by only considering FWF effect on the ocean through the SSS pathway.

Figure 16 shows percentage changes in standard deviations of the Niño 3.4 SST, SSS, Q_B, and MLD anomalies as a function of the calendar month. When only considering interannual FWF effect through SSS pathway, the percentages increase in standard deviation of the Niño 3.4 anomalies for SST, SSS, Q_B and MLD account for about 80%, 75%, 80%, and 80% (except for in April, October and November, which accounts for about 60%), respectively. In more details,

SST Standerd Deviation

(a) FWF(Sinter, Binter)

(b) FWF(Sclim, Bclim)

(c) FWF(Sinter, Bclim)
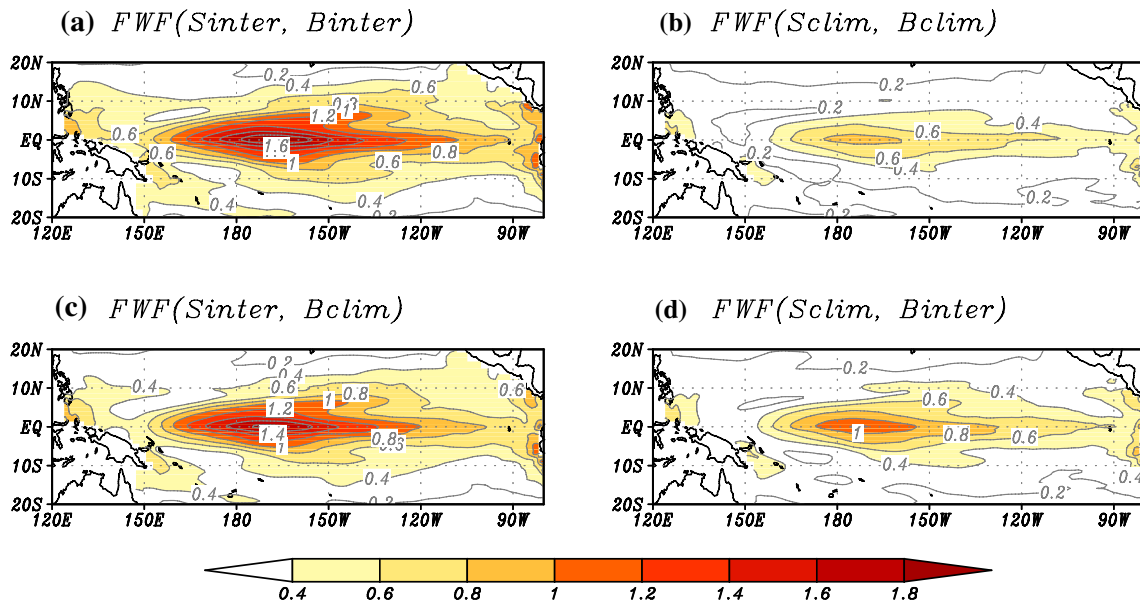
(d) FWF(Sclim, Binter)

Fig. 12 Maps for standard deviations of SST anomalies calculated from the last 80-year simulation in **a** FWF(S_{inter}, B_{inter}), **b** FWF(S_{clim}, B_{clim}), **c** FWF(S_{inter}, B_{clim}), and **d** FWF(S_{clim}, B_{inter}). The contour interval is 0.2 °C
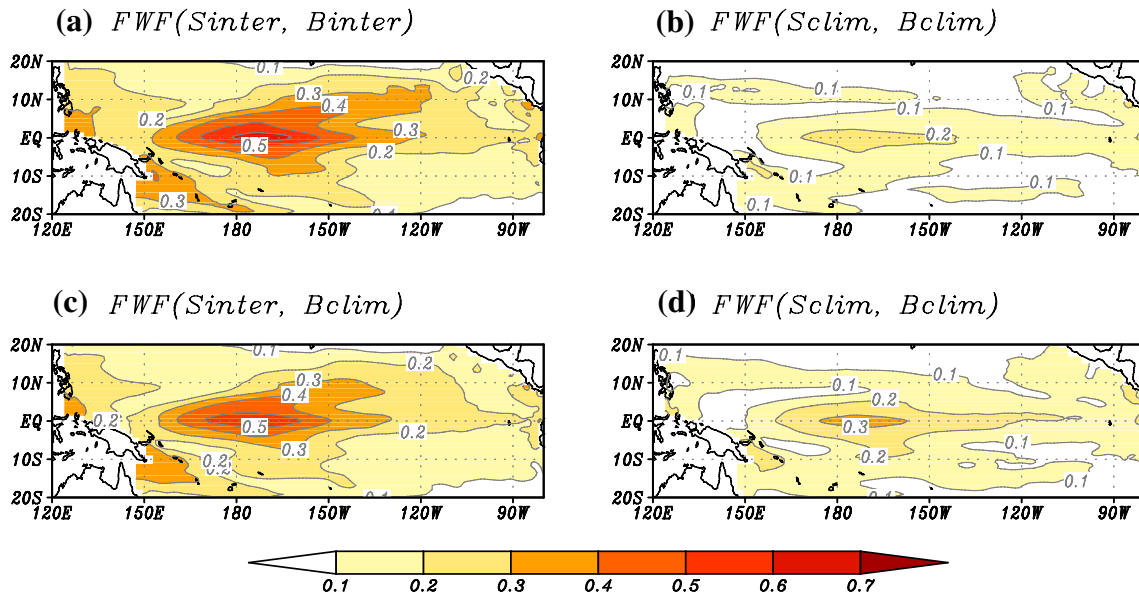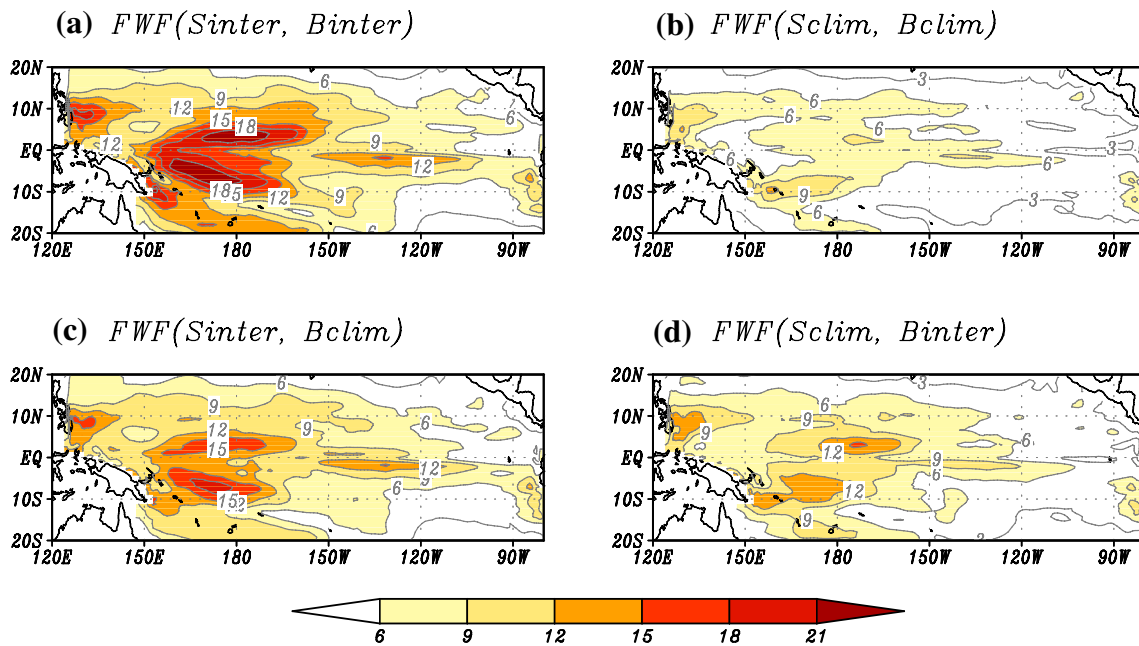
SSS Standerd Deviation

(a) FWF(Sinter, Binter)

(b) FWF(Sclim, Bclim)

(c) FWF(Sinter, Bclim)
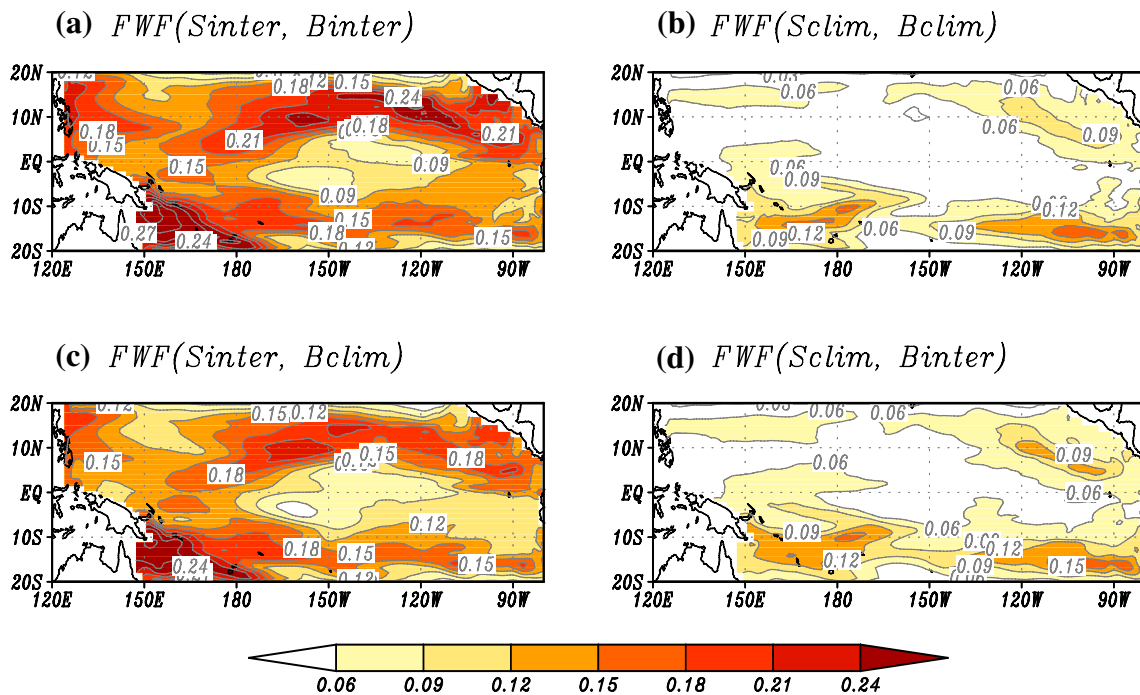
(d) FWF(Sclim, Binter)

Fig. 13 Maps for standard deviations of SSS anomalies calculated from the last 80-year simulation in **a** FWF(S_{inter}, B_{inter}), **b** FWF(S_{clim}, B_{clim}), **c** FWF(S_{inter}, B_{clim}), and **d** FWF(S_{clim}, B_{inter}). The contour interval is 0.03 psu

Fig. 14 Maps for standard deviations of Q_B anomalies calculated from the last 80-year simulation in **a** FWF(S_{inter}, B_{inter}), **b** FWF(S_{clim}, B_{clim}), **c** FWF(S_{inter}, B_{clim}), and **d** FWF(S_{clim}, B_{inter}). The contour interval is 0.1×10^{-6} kg s^{-1} m^{-2}

Fig. 15 Maps for standard deviations of MLD anomalies calculated from the last 80-year simulation in **a** FWF(S_{inter}, B_{inter}), **b** FWF(S_{clim}, B_{clim}), **c** FWF(S_{inter}, B_{clim}), and **d** FWF(S_{clim}, B_{inter}). The contour interval is 3 m

the standard deviations of some specific anomaly fields are shown in Table 2. For example, the standard deviation of Niño3 and Niño4 SST anomalies are 0.93 °C and 1.32 °C in

FWF(S_{inter}, B_{inter}), 0.83 °C and 1.23 °C in FWF(S_{inter}, B_{clim}), and 0.5 °C and 0.62 °C in FWF(S_{clim}, B_{clim}), respectively. Compared with FWF(S_{clim}, B_{clim}), these values represent

increases of about 86% (113%) for the Niño3 (Niño4) SST variability in FWF(S_{inter}, B_{inter}), and about 66% (98%) for the Niño3 (Niño4) SST variability in FWF(S_{inter}, B_{clim}), respectively. The percentage increase of the standard deviation of Niño3 (Niño4) SST anomalies in FWF(S_{inter}, B_{clim}) relative to that in FWF(S_{inter}, B_{inter}) is about 77% (87%). In addition, the percentage increase of the standard deviation of Niño4 SSS anomalies in FWF(S_{inter}, B_{clim}) relative to that in FWF(S_{inter}, B_{inter}) is 78%; the percentage increase of the standard deviation of Niño4 Q_B anomalies in FWF(S_{inter}, B_{clim}) relative to that in FWF(S_{inter}, B_{inter}) is 86%; the percentage increase of the standard deviation of

Niño4 MLD anomalies in FWF(S_{inter}, B_{clim}) is 60% relative to that in FWF(S_{inter}, B_{inter}). All these values show that the ENSO amplitude increases in FWF(S_{inter}, B_{clim}) relative to FWF(S_{clim}, B_{clim}), which is mainly attributed to the SSS pathway.

4.2 The Q_B influence pathway

Another influence pathway associated with interannual FWF variability on ENSO is through Q_B and the related results are illustrated in this subsection. Firstly, modulations of interannual FWF variability effect through the Q_B pathway on
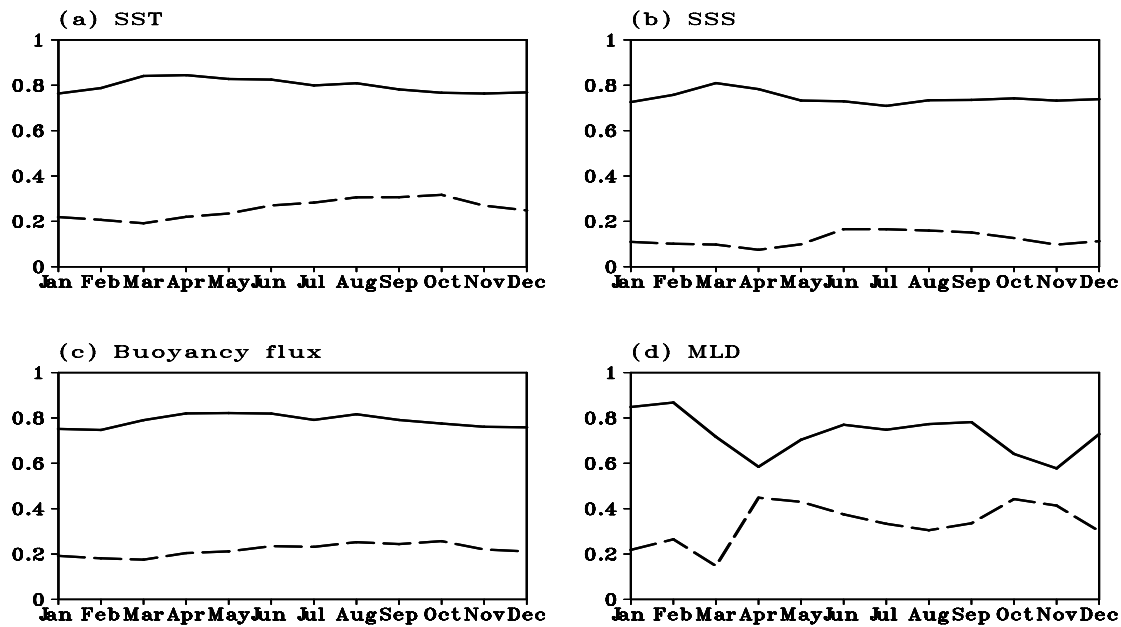
Fig. 16 Percentage changes in standard deviations of the Niño 3.4 **a** SST, **b** SSS, **c** Q_B, and **d** MLD anomalies as a function of the calendar month calculated from the last 80-year simulation. The solid line is calculated by the percentage of the difference between FWF(S_{inter}, B_{clim}) and FWF(S_{clim}, B_{clim}) relative to the difference between FWF(S_{inter}, B_{inter}) and FWF(S_{clim}, B_{clim}), and the long dash line is calculated by the percentage of the difference between FWF(S_{clim}, B_{inter}) and FWF(S_{clim}, B_{clim}) relative to the difference between FWF(S_{inter}, B_{inter}) and FWF(S_{clim}, B_{clim})

Table 2 The standard deviations of some specific anomaly fields simulated in the four experiments described in Table 1

	FWF(S_{inter}, B_{inter})	FWF(S_{inter}, B_{clim})	FWF(S_{clim}, B_{inter})	FWF(S_{clim}, B_{clim})
Niño 4 SST	1.32	1.23	0.82	0.62
Niño 4 FWF	157.45	142.02	94.58	0
Niño 4 SSS	0.14	0.12	0.06	0.05
Niño 4 Q_B	0.46	0.42	0.24	0.18
Niño 4 MLD	16.44	12.68	10.53	7.16
Niño 4 τ_x	0.28	0.25	0.16	0.12
Niño 3 SST	0.93	0.83	0.61	0.50
Niño 1 + 2 SST	0.80	0.74	0.57	0.47

Results shown are SST, FWF, SSS, Q_B, MLD and τ_x at the Niño 4 region; the Niño 3 SST and the Niño 1 + 2 SST, which are calculated from the last 80-year simulation. The units are °C for SST, mm month^{-1} for FWF, psu for SSS, 10^{-6} kg s^{-1} m^{-2} for Q_B, m for MLD and dyn cm^{-2} for τ, respectively

interannual variations are demonstrated, and then, quantitative assessments in ENSO amplitude are given.

The interannual FWF anomalies along the equator during the model 21–40-year simulation in $FWF(S_{clim}, B_{inter})$ are show in Fig. 5c. The simulated maximum interannual FWF amplitude is about 200 mm month^{-1} during ENSO peak stage. It is much weaker compared with $FWF(S_{inter}, B_{inter})$ (Fig. 5a), also weaker than $FWF(S_{inter}, B_{clim})$ (Fig. 5a). As analyzed above, only considering the interannual FWF effect through Q_B pathway, the interannual FWF anomalies can be underestimated compared with the interannual FWF effect both through SSS and Q_B pathways. However, the interannual variations of FWF in $FWF(S_{inter}, B_{inter})$ are not equal to the sum of those in $FWF(S_{inter}, B_{clim})$ and $FWF(S_{clim}, B_{inter})$, suggesting a role played by nonlinear effects induced by FWF forcing to the ocean.

The interannual SST anomalies show a coherent structure and temporal variation with FWF. When only interannual FWF variability effect on Q_B is represented in $FWF(S_{clim}, B_{inter})$, ENSO signal is stronger compared with that in $FWF(S_{clim}, B_{clim})$, with the amplitude about 1.5 °C (Fig. 6d). But it is weaker than that in $FWF(S_{inter}, B_{inter})$, even weaker than that in $FWF(S_{inter}, B_{clim})$. Because the SSS variability is directly influenced by interannual FWF variability, only interannual FWF effect through Q_B pathway represented contributes to a weak effect on simulated SSS variability. The strength of interannual SSS variability in $FWF(S_{clim}, B_{inter})$ (Fig. 7d) is more or less the same as in $FWF(S_{clim}, B_{clim})$ (Fig. 7b), with the amplitude being about 0.08 psu. The strength of interannual SSS variability in $FWF(S_{clim}, B_{inter})$ is obviously much weaker than that in $FWF(S_{inter}, B_{clim})$. It illustrates that through the Q_B pathway, interannual FWF variability has a small impact on interannual SSS variability.

The interannual Q_B variations along the equator are shown in Fig. 8. When only the interannual FWF effect on Q_B pathway is represented in $FWF(S_{clim}, B_{inter})$, the amplitude of Q_B anomaly is about 0.4×10^{-6} kg s^{-1} m^{-2}, which is much weaker than that in $FWF(S_{inter}, B_{inter})$. As shown in Eq. (1), buoyancy flux consists of heat flux and freshwater flux. Here, the amplitude of Q_S is weaker than Q_T, and so Q_S plays a compensation role in Q_B compared with Q_T, which plays a major role in Q_B (Zhang and Busalacchi 2009b). Thus, even interannual FWF effect through Q_B pathway is not directly represented, the amplitude of Q_B anomalies in $FWF(S_{inter}, B_{clim})$ is still larger than that in $FWF(S_{clim}, B_{inter})$. It is mainly because the major role of heat flux is playing in Q_B. MLD is directly affected by Q_B, and these two fields are of the same sign. The interannual MLD anomalies along the equator are shown in Fig. 9, with the shoaled (deepened) mixed layer during El Niño (La Niña) phase. The ENSO related interannual FWF variability tends to reinforce the zonal seesaw pattern of MLD anomalies. In $FWF(S_{clim},$

$B_{inter})$, the maximum MLD anomaly value of the zonal seesaw pattern is 16 m (Fig. 8d), which is stronger than that in $FWF(S_{clim}, B_{clim})$, but weaker than that in $FWF(S_{inter}, B_{inter})$, even weaker than that in $FWF(S_{inter}, B_{clim})$.

These related oceanic processes in turn affect SST, which are consistent with SST variations shown in Fig. 6. The anomaly amplitude of the Niño3.4 SST time series in $FWF(S_{clim}, B_{inter})$ is smaller than that in $FWF(S_{inter}, B_{inter})$, even smaller than that in $FWF(S_{inter}, B_{clim})$ (Fig. 4). This illustrates that the effects of interannual FWF variability on ENSO are mainly realized through SSS pathway; the Q_B pathway plays a compensatory role. If the FWF forcing effects are not represented fully in the ocean model (such as level ocean model), the FWF positive feedback on ENSO can be underestimated.

When only interannual FWF effect through Q_B pathway is represented, the maximum SST variation value is about 1.0 °C, centered in the central equatorial Pacific (Fig. 12d), which is larger than that in $FWF(S_{clim}, B_{clim})$. The standard deviations of the Niño 3.4 SST anomalies as a function of the calendar month are shown in Fig. 10. The standard deviation of the Niño 3.4 SST anomalies in $FWF(S_{clim}, B_{inter})$, with the maximum value about 0.9 °C in May, is much smaller than that in $FWF(S_{inter}, B_{inter})$, even smaller than that in $FWF(S_{inter}, B_{clim})$. It shows that interannual FWF effect through the SSS pathway can induce larger SST variations than that through the Q_B pathway. However, the intensity of interannual SST anomalies affected by interannual FWF effect through each pathway is larger than that when FWF is prescribed as seasonally varying climatology, and smaller than that when interannual FWF effects through SSS and Q_B pathways are both represented. These two sensitivity experiments both underestimate the strength of SST variation compared with the simulations in which both interannual FWF effects through SSS and Q_B pathways are represented.

We can compare other fields in $FWF(S_{clim}, B_{inter})$ with other experiments. For example, the maximum value of FWF variability in $FWF(S_{clim}, B_{inter})$ is 120 mm month^{-1}, centered in the central tropical Pacific near the dateline, which is smaller than that in $FWF(S_{inter}, B_{inter})$ and $FWF(S_{inter}, B_{clim})$, respectively (Fig. 11). It is clear that interannual FWF effect through Q_B pathway serves a positive feedback on ENSO. However, the strength of feedback is weaker than that in which interannual FWF effect is represented through SSS pathway.

Directly affected by FWF, the intensity of SSS variation in $FWF(S_{clim}, B_{inter})$ (Fig. 13d) is almost the same as that in $FWF(S_{clim}, B_{clim})$ (Fig. 13b); they are both much smaller than that in $FWF(S_{inter}, B_{inter})$ and $FWF(S_{inter}, B_{clim})$. Another variable directly affected by FWF is Q_B, whose maps for standard deviations are shown in Fig. 14. The maximum value of Q_B variation in $FWF(S_{clim}, B_{inter})$ is only about 0.3×10^{-6} kg s^{-1} m^{-2}, centered in the central tropical Pacific

(Fig. 14d). It is slightly larger than that in FWF(S_{clim}, B_{clim}) (about 0.2×10^{-6} kg s^{-1} m^{-2}; Fig. 14b), but much smaller than that in FWF(S_{inter}, B_{inter}) (0.6×10^{-6} kg s^{-1} m^{-2}; Fig. 14a) and FWF(S_{inter}, B_{clim}) (0.5×10^{-6} kg s^{-1} m^{-2}; Fig. 14c). These are mainly because the heat flux plays a major role in Q_B, whereas the freshwater flux plays a compensatory role in contributing to Q_B anomalies.

MLD is calculated using the bulk mixed layer model in which wind stress and buoyancy flux are explicitly making contributing to variations in MLD. As a part of Bjerknes feedback (Bjerknes 1969), MLD variations play an important role in ENSO cycles. When only interannual FWF effect through Q_B pathway is represented, the maximum value of MLD variation is about 15 m (located in the north extratropics of the central basin; Fig. 15d). It is much smaller than that in FWF(S_{inter}, B_{inter}).

The percentage changes in standard deviations of the related ocean variables in Niño 3.4 area are calculated to quantitatively assess changes in ENSO amplitude induced through Q_B pathway. That is, the percentage of the difference between FWF(S_{clim}, B_{inter}) and FWF(S_{clim}, B_{clim}) relative to that between FWF(S_{inter}, B_{inter}) and FWF(S_{inter}, B_{clim}) is calculated to represent the increases in amplitude, which is shown in Fig. 16. When only interannual FWF effect through Q_B pathway is represented, the percentage increase in standard deviation of the Niño 3.4 SSS anomalies accounts for about more than 20%, even more than 30% especially from August to October; the percentage increase in standard deviation of the Niño 3.4 SSS and Q_B anomalies accounts respectively for about 10% and 20%, with slightly variations in different months; the percentage increase in standard deviation of the Niño 3.4 MLD anomalies accounts for about 40%, except for from January to March (accounts for about 20%). In general, the increase in ENSO amplitude in FWF(S_{clim}, B_{inter}) plays a compensatory role compared with the contribution of FWF(S_{inter}, B_{clim}) relative to FWF(S_{inter}, B_{inter}). However, the sum of the increased percentage values for the corresponding variables in Niño 3.4 area between FWF(S_{inter}, B_{clim}) and FWF(S_{clim}, B_{inter}) relative to FWF(S_{inter}, B_{inter}) are not linearly equal to 100%.

Further focused analyses on the standard deviations of some specific anomaly fields are shown in Table 2. For example, the standard deviations of Niño3 and Niño4 SST anomalies are 0.61 °C and 0.82 °C in FWF(S_{clim}, B_{inter}). Compared with FWF(S_{clim}, B_{clim}), the percentage increase for FWF(S_{clim}, B_{inter}) in the standard deviation of Niño3 (Niño4) SST anomalies relative to FWF(S_{inter}, B_{inter}) is 26% (28%). In addition, the percentage increase for FWF(S_{clim}, B_{inter}) in the standard deviation of Niño4 SSS anomalies relative to FWF(S_{inter}, B_{inter}) is 11%; the percentage increase for FWF(S_{clim}, B_{inter}) in the standard deviation of Niño4 Q_B anomalies relative to FWF(S_{inter}, B_{inter}) is 21%; the percentage increase for FWF(S_{clim}, B_{inter}) in the standard deviation

of Niño4 MLD anomalies relative to FWF(S_{inter}, B_{inter}) is 36%. All these values for FWF(S_{inter}, B_{inter}) show that the increase in ENSO amplitude is not a simply linear summation of that in FWF(S_{inter}, B_{clim}) and FWF(S_{clim}, B_{inter}) relative to FWF(S_{clim}, B_{clim}). Moreover, different ocean process contributions due to differently represented interannual FWF effects are not the same.

5 Summary and discussion

FWF is one of major atmospheric forcings to the ocean, but has been received less attention than surface fluxes of momentum (wind stress) and heat. Currently, there exist large model biases induced by the ways FWF is represented in climate models. Previous studies have illustrated ENSO modulations due to interannual variability of FWF in the tropical Pacific using a hybrid coupled model. Interannual FWF variability is demonstrated to have a positive feedback on ENSO. During El Niño event, there is a warm SST anomaly in the central and eastern tropical Pacific, along with a positive FWF anomaly in the western basin. The positive FWF anomaly can directly affect salinity in the upper ocean and buoyance flux at the sea surface, reducing mixed layer salinity with more stable vertical stratification, and thus reduce vertical mixing. In addition, the positive FWF anomaly (the ocean receives freshwater) makes the surface layer less buoyant, with reduced buoyancy force and more negative Q_B anomaly, which acts to produce a shoaled mixed layer and reduced entrainment of subsurface water into the mixed layer. These interrelationships among the related ocean processes further strengthen the warm SST anomaly, serving as a positive feedback on ENSO. In the coupled system, the atmospheric FWF variability can have a strong influence on the ocean state, including SST. The changes in SST in turn affect the atmospheric wind through air-sea interactions. Then, the FWF and wind forcings are acting together to affect ENSO.

Physically, there are two pathways by which FWF can affect the ocean: one through SSS, and the other through Q_B. In this work, the roles played by interannual FWF variability in modulating ENSO through its effects either on SSS or Q_B pathways are separately and quantitatively examined using a hybrid coupled model (HCM) of the tropical Pacific; its ocean component used is a sigma coordinate layer model in which the topmost layer is treated as a mixed layer whose depth is a prognostic variable. A bulk ML model is embedded into the OGCM with varying ML depth that is explicitly and directly affected by Q_B. Four HCM-based sensitivity experiments with differently represented FWF effects are designed using the coupled system to illustrate the roles the two pathways played in ENSO modulations, with SSS and Q_B being affected individually or collectively.

A corresponding feedback process induced by interannual FWF effect can be traced from these experiments. Results show that a positive feedback on ENSO is induced by interannual FWF variability through the two pathways and the feedback intensities on ENSO differ among modeling experiments with differently represented FWF effects. The largest anomalies are produced when interannual FWF effects on SSS and Q_B are both represented compared with other cases. Furthermore, anomalies produced by only interannual FWF effect through SSS pathway is larger than that by only interannual FWF effect through Q_B pathway; both are smaller than that when interannual FWF effects through SSS and Q_B pathways are both represented.

The increases in ENSO amplitude by the differently represented FWF effect on the ocean through the two pathways of SSS and Q_B are quantified. Results show that the ENSO amplitude in $FWF(S_{inter}, B_{clim})$ accounts for about 80% compared with that in $FWF(S_{inter}, B_{inter})$, whereas that in $FWF(S_{clim}, B_{inter})$ accounts for about 20%. This illustrates that the effects of interannual FWF variability on interannual variations in the tropical Pacific climate system are mainly realized through the SSS pathway. If the FWF effects are not fully represented in the ocean model (as in the case for the level ocean model), the effect of FWF-induced positive feedback on ENSO can be underestimated. In addition, the increase in ENSO amplitude produced by both interannual FWF effects through SSS and Q_B pathways is not a simply linear summation of that produced individually through SSS pathway or Q_B pathway alone, indicating a nonlinear adjustment in the ocean.

This study provides a new insight into the model biases associated with FWF effects in the tropical Pacific; the results are useful not only in terms of a physical understanding of differently represented FWF forcing on the ocean dynamics and ENSO, but also in terms of the improvements in coupled models. It is clearly evident that the contribution to buoyancy flux from interannual FWF variability plays a certain role in the mixed layer and the strength of positive feedback on ENSO. When the related ocean processes in the ocean models are neglected (i.e., as in level ocean models), the corresponding positive feedback effect can be underestimated on ENSO. Here, we only demonstrate the effects of differently represented FWF forcing on ENSO simulations; its effects on ENSO prediction and predictability need to be investigated further.

References

Bjerknes J (1969) Atmospheric teleconnections from the equatorial Pacific. Mon Weather Rev 97(3):163–172

Capotondi A, Wittenberg AT, Newman M et al (2015) Understanding ENSO diversity. Bull Am Meteor Soc 96(6):921–938

Chen D, Lian T, Fu C et al (2015) Strong influence of westerly wind bursts on El Niño diversity. Nat Geosci 8(5):339

Chen D, Rothstein LM, Busalacchi AJ (1994) A hybrid vertical mixing scheme and its application to tropical ocean models. J Phys Oceanogr 24(10):2156–2179

Cravatte S, Delcroix T, Zhang D et al (2009) Observed freshening and warming of the western Pacific warm pool. Clim Dyn 33(4):565–589

Delcroix T, Alory G, Cravatte S, Corrège T, McPhaden MJ (2011) A gridded sea surface salinity data set for the tropical Pacific with sample applications (1950–2008). Deep Sea Res Part I 58(1):38–48

Gent PR, Cane MA (1989) A reduced gravity, primitive equation model of the upper equatorial ocean. J Comput Phys 81(2):444–480

Kang X, Zhang RH (2017) Effects of different freshwater flux representations in an ocean general circulation model of the tropical Pacific. Sci Bull 62(5):345–351

Karnauskas KB, Busalacchi AJ (2009) Mechanisms for the interannual variability of SST in the east Pacific warm pool. J Clim 22(6):1375–1392

Karnauskas KB, Busalacchi AJ, Murtugudde R (2008) Low-frequency variability and remote forcing of gap winds over the east Pacific warm pool. J Clim 21(19):4901–4918

Kessler WS (1999) Interannual variability of the subsurface high salinity tongue south of the equator at 165 E. J Phys Oceanogr 29(8):2038–2049

Kraus EB, Turner JS (1967) A one-dimensional model of the seasonal thermocline II: The general theory and its consequences. Tellus 19(1):98–106

Large WG, McWilliams JC, Doney SC (1994) Oceanic vertical mixing: a review and a model with a nonlocal boundary layer parameterization. Rev Geophys 32(4):363–403

Latif M, Keenlyside NS (2009) El Niño/Southern Oscillation response to global warming. Proc Natl Acad Sci 106(49):20578–20583

Lumpkin R, Speer K (2007) Global ocean meridional overturning. J Phys Oceanogr 37(10):2550–2562

Lupton JE, Delaney JR, Johnson HP et al (1985) Entrainment and vertical transport of deep-ocean water by buoyant hydrothermal plumes. Nature 316(6029):621

Maes C, Picaut J, Belamari S (2002) Salinity barrier layer and onset of El Nino in a Pacific coupled model. Geophys Res Lett 29(24):1–4

Miller JR (1976) The salinity effect in a mixed layer ocean model. J Phys Oceanogr 6(1):29–35

Murtugudde R, Seager R, Busalacchi A (1996) Simulation of the tropical oceans with an ocean GCM coupled to an atmospheric mixed-layer model. J Clim 9(8):1795–1815

Price JF, Weller RA, Pinkel R (1986) Diurnal cycling: Observations and models of the upper ocean response to diurnal heating, cooling, and wind mixing. J Geophys Res Oceans 91(C7):8411–8427

Qu T, Song YT, Maes C (2014) Sea surface salinity and barrier layer variability in the equatorial Pacific as seen from Aquarius and Argo. J Geophys Res Oceans 119(1):15–29

Ren HL, Zuo J, Jin FF et al (2016) ENSO and annual cycle interaction: the combination mode representation in CMIP5 models. Clim Dyn 46(11–12):3753–3765

Seager R, Blumenthal MB, Kushnir Y (1995) An advective atmospheric mixed layer model for ocean modeling purposes: global simulation of surface heat fluxes. J Clim 8(8):1951–1964

Vialard J, Delecluse P (1998) An OGCM study for the TOGA decade. Part I: Role of salinity in the physics of the western Pacific fresh pool. J Phys Oceanogr 28(6):1071–1088

Vialard J, Delecluse P, Menkes C (2002) A modeling study of salinity variability and its effects in the tropical Pacific Ocean during the 1993–1999 period. J Geophys Res Oceans 107(C12):1–14

Waliser DE, Somerville RC (1994) Preferred latitudes of the intertropical convergence zone. J Atmos Sci 51(12):1619–1639

Willebrand J (1993) Forcing the ocean by heat and freshwater fluxes, energy and water cycles in the climate system. Springer, Berlin, pp 215–233

Wu L, Sun Y, Zhang J et al (2010) Coupled ocean–atmosphere response to idealized freshwater forcing over the western tropical Pacific. J Clim 23(7):1945–1954

Xie SP, Philander SG (1994) A coupled ocean-atmosphere model of relevance to the ITCZ in the eastern Pacific. Tellus A 46(4):340–350

Zhang RH (2015) Structure and effect of ocean biology-induced heating (OBH) in the tropical Pacific, diagnosed from a hybrid coupled model simulation. Clim Dyn 44(3–4):695–715

Zhang RH, Busalacchi AJ (2009a) Freshwater flux (FWF)-induced oceanic feedback in a hybrid coupled model of the tropical Pacific. J Clim 22(4):853–879

Zhang RH, Busalacchi AJ (2009b) An empirical model for surface wind stress response to SST forcing induced by tropical instability waves (TIWs) in the eastern equatorial Pacific. Mon Weather Rev 137(6):2021–2046

Zhang RH, Busalacchi AJ, Murtugudde RG (2006) Improving SST anomaly simulations in a layer ocean model with an embedded entrainment temperature submodel. J Clim 19(18):4638–4663

Zhang RH, Gao C (2016) The IOCAS intermediate coupled model (IOCAS ICM) and its real-time predictions of the 2015–2016 El Niño event. Sci Bull 61(13):1061–1070

Zhang RH, Gao C, Kang X et al (2015) ENSO modulations due to interannual variability of freshwater forcing and ocean biology-induced heating in the tropical Pacific. Sci Rep 5:18506

Zhang RH, Tian F, Busalacchi AJ et al (2019) Freshwater flux and ocean chlorophyll produce nonlinear feedbacks in the tropical Pacific. J Clim 32(7):2037–2055

Zhang RH, Zebiak SE (2002) Effect of penetrating momentum flux over the surface boundary/mixed layer in a z-coordinate OGCM of the tropical Pacific. J Phys Oceanogr 32(12):3616–3637

Zhang RH, Zebiak SE (2004) An embedding method for improving interannual variability simulations in a hybrid coupled model of the tropical Pacific ocean–atmosphere system. J Clim 17(14):2794–2812

Zhang RH, Zheng F, Zhu J et al (2012) Modulation of El Niño-Southern Oscillation by freshwater flux and salinity variability in the tropical Pacific. Adv Atmos Sci 29(4):647–660

Zheng F, Zhang RH (2015) Interannually varying salinity effects on ENSO in the tropical Pacific: a diagnostic analysis from Argo. Ocean Dyn 65(5):691–705

Zhi H, Zhang RH, Lin P et al (2015) Quantitative analysis of the feedback induced by the freshwater flux in the tropical Pacific using CMIP5. Adv Atmos Sci 32(10):1341–1353

Zhu J, Huang B, Zhang RH et al (2014) Salinity anomaly as a trigger for ENSO events. Sci Rep 4:6821

Zhu Y, Zhang RH (2018) Scaling wind stirring effects in an oceanic bulk mixed layer model with application to an OGCM of the tropical Pacific. Clim Dyn 51(5–6):1927–1946